

Convective vortices and dust devils detected and characterized by Mars 2020

R. Hueso¹, C. E. Newman², T. del Río-Gaztelurrutia¹, A. Munguira¹, A. Sánchez-Lavega¹, D. Toledo³, V. Apéstigue³, I. Arruego³, A. Vicente-Retortillo⁴, G. Martínez⁵, M. Lemmon⁶, R. Lorenz⁷, M. Richardson², D. Viudez-Moreiras⁵, M. de la Torre-Juarez⁸, J. A. Rodríguez-Manfredi⁵, L. K. Tamppari⁶, N. Murdoch⁹, S. Navarro-López⁵, J. Gómez-Elvira⁵, M. Baker¹⁰, J. Pla-García⁵, A. M. Harri¹¹, M. Hietala¹¹, M. Genzer¹¹, J. Polkko¹¹, I. Jaakonaho¹¹, T. Mäkinen¹¹, A. Stott⁷, D. Mimoun⁷, B. Chide¹², E. Sebastian⁵, D. Banfield¹³, and A. Lepinette-Malvite⁵

¹Física Aplicada, Escuela de Ingeniería de Bilbao, Universidad del País Vasco UPV/EHU, Bilbao, Spain

²Aeolis Research, Chandler, AZ, USA

³Instituto Nacional de Técnica Aeroespacial (INTA), Madrid, Spain

⁴Centro de Astrobiología (INTA-CSIC), Madrid, Spain

⁵Lunar and Planetary Institute, Houston, TX, USA

⁶Space Science Institute, College Station, TX, USA

⁷Johns Hopkins Applied Physics Laboratory, Laurel, MD, USA

⁸Jet Propulsion Laboratory, California, USA

⁹Institut Supérieur de l'Aéronautique et de l'Espace (ISAE-SUPAERO), Université de Toulouse, Toulouse, France

¹⁰Smithsonian Institution, Washington, DC, USA

¹¹Finnish Meteorological Institute, Helsinki, Finland

¹²Los Alamos National Laboratory, Los Alamos, NM, USA

¹³Cornell Center for Astrophysics and Planetary Science, Cornell University, Ithaca, NY, USA

Key Points:

- Vortices and dust devils are frequent on Jezero. MEDA detects 5.0 and 1.0 events per sol respectively when correcting from sampling effects.
- Intense vortices on Jezero tend to be dusty with 66% of all vortices with a pressure drop larger than 2.0 Pa being dusty.
- We calculate 2.5 and 0.1 dust devils $\text{km}^{-2}\text{sol}^{-1}$ with sizes of 20 m and 100 m respectively. The largest events dominate dust lifting.

Corresponding author: R. Hueso, Ricardo.Hueso@ehu.eus

Abstract

We characterize the vortex and dust devil activity at Jezero from pressure and winds obtained with the MEDA instrument on Mars 2020 over 415 sols ($L_s=6-213^\circ$). Vortices are abundant (4.9 vortices per sol with pressure drops >0.5 Pa when correcting from gaps in coverage) and peak at noon. At least one in every 5 vortices carries dust from RDS-MEDA data, and intense vortices are more likely to carry dust. Seasonal variability was small but dust devils were abundant during a dust storm ($L_s=152-156^\circ$). Vortices are more frequent and intense over terrains with lower thermal inertia favoring a higher daytime surface-to-air temperature gradient. We fit measurements of wind and pressure during dust devil encounters to models of vortices, and investigate their physical characteristics. Diameters range from 5 to 135 m with a mean of 20 m. Three 100-m size events passed within 30 m of the rover. From the close encounters we estimate a dust devil activity of 2.0-3.0 dust devils $\text{km}^{-2} \text{sol}^{-1}$. A comparison of MEDA observations with a Large Eddy Simulation of Jezero at $L_s=45^\circ$ produces a similar result. We estimate that large dust devils with diameters >100 m have a density of 0.1 dust devils $\text{km}^{-2}\text{sol}^{-1}$, implying that dust lifting is dominated by the largest vortices in the region. At least one vortex had a central pressure drop of 9.0 Pa and internal winds of 25 ms^{-1} . The MEDA wind sensors were partially damaged during two dust devil encounters, and we detail these events.

Plain Language Summary

Dust devils are whirlwinds of warm air with winds strong enough to lift dust. They are common in Earth deserts and much more abundant on Mars, where they are one of the elements that bring dust to the atmosphere. The Mars 2020 mission landed in Jezero crater on February 2020 and has observed a plethora of dust devils that we investigate with the meteorological sensors on the MEDA instrument. Results for more than 400 Martian days from Spring to Autumn indicate a high abundance of events with small seasonal variability. Terrains with lower thermal inertia warming more efficiently at noon favor the appearance of dust devils. We also found an increased dust devil activity during a short dust storm that covered the region. From modeling MEDA data we find that dust devils at Jezero have diameters from 5.0 to 135 m. We estimate that about 2-3 dust devils are formed per km^2 and sol. Large vortices with diameters of 100 m form frequently enough to dominate dust lifting at Jezero. Two dust devils damaged part of the hardware of the wind sensors of MEDA and we detail the characteristics of those events.

1 Introduction

Daytime convective vortices are common on Mars and Earth (Balme & Greeley, 2006). They constitute one of the various phenomena that develop in the Planetary Boundary Layer (PBL) of both planets, but are much more common and can be far larger on Mars due to the more extended PBL depth. Dusty convective vortices or Dust Devils (DDs) are vortices that have raised dust from the surface, via the combination of tangential winds around the vortex, central pressure drop and electrostatic forces between dust grains (Neakrase et al., 2016). DDs constitute an important element of the Martian atmospheric dust cycle thought to account for a significant part of the background dust haze on Mars (Newman et al., 2002; Basu et al., 2004; Kahre et al., 2006, 2017). In addition, DDs can change the local albedo creating Dust Devil Tracks (DDTs) (Fenton et al., 2016; Reiss et al., 2016) and can also ‘clean’ dust off spacecraft surfaces (Vicente-Retortillo et al., 2018), including solar panels (R. D. Lorenz & Reiss, 2015), enabling solar-powered missions to last longer. Conversely, dust grains carried by the strong vortex winds can represent a hazard to surface hardware (Balme & Greeley, 2006). Thus, characterizing the dust devil activity at Jezero, the location of

the Mars 2020 mission, which is collecting the first samples of Mars to be brought to Earth (Farley et al., 2020), is important for understanding risks to the landed elements involved in the Mars Sample Return mission.

Field data obtained by meteorological sensors can characterize the physical properties of convective vortices and imaging instruments can also determine many of the properties of DDs (Murphy et al., 2016). Vortices can be identified in dips in the pressure record and in sharp changes in wind intensity and direction (Ryan & Lucich, 1983). Vortices also produce warmer temperatures at their core, and the presence of dust can be investigated with photodiodes (Mason et al., 2013; Ordóñez-Etxeberria et al., 2020; Kahanpää & Viúdez-Moreiras, 2021).

The MEDA instrument on the Mars 2020 Perseverance rover carries sensors capable of simultaneously obtaining all those measurements (Rodríguez-Manfredi et al., 2021). MEDA measures air pressure and horizontal winds that can be used to determine the physical properties of the vortices. The Radiation and Dust Sensors (RDS) on MEDA are a set of photodiodes oriented at different directions including a panchromatic sensor pointing to the vertical (RDS Top 7) with a 90° Field of View (Apestigue et al., 2022). On Earth and Mars the near surface temperature lapse rate is a key element in determining the frequency, intensity, and horizontal size and vertical extension of the vortices (Ryan, 1972; Rennó et al., 1998; Ordóñez-Etxeberria et al., 2020; Spiga et al., 2021). MEDA measures the ground temperature and air temperatures at different altitudes using the Thermal InfraRed Sensors (TIRS) and Air Temperature Sensors (ATS) packages (Rodríguez-Manfredi et al., 2021, 2022; Munguira et al., 2022). Thus, multi-sensorial investigations of convective vortices and DDs and the properties of the environment in which they develop are possible with MEDA.

The Mars 2020 Perseverance rover landed on Mars in Jezero crater at 77.5°E and 18.4°N at Ls=6.2° (North hemisphere Spring). Predictions before landing based on Mars atmospheric models suggested that Jezero is a location where intense vortices form regularly, peaking in activity at Ls~ 120° (Newman et al., 2021). Jackson (2022) performed an initial analysis of MEDA pressure and RDS data in the first 89 sols of the mission, finding a high frequency of vortices and high rate of DDs. A more extensive analysis up to mission sol 216 (covering early spring through early summer), which also examined DDs in Mars 2020 imaging instruments, found that on average over four vortices passed the rover per sol, at least a quarter of which were dusty (Newman et al., 2022). The same study showed a positive correlation between vortex intensity (in terms of the measured pressure drop and wind speed) and dust lifting (in terms of vortex dust content and local surface dust removal).

The abundance of DDs at Jezero has a stark contrast with the lack of them in Elysium Planitia, where the Insight mission has detected thousands of vortices (Banfield et al., 2020; Spiga et al., 2021; Chatain et al., 2021) with no dust activity (Lorenz et al. 2021). Following arguments presented by Spiga et al. (2021) of vortex abundance being influenced by environment winds, Newman et al. (2022) concluded that the intrinsic activity of vortices at Elysium Planitia and Jezero is very similar over spring and early summer, but the stronger winds at Elysium advected vortices more rapidly over the sensors, resulting in nearly double the number of detections. Differences in the DD abundance are most likely due to distinct surface properties, including the different availability at the surface of mobile dust particles.

Here we extend the vortex and DD results presented in Newman et al. (2022) to cover the first 415 sols of the mission up to Ls=213° (northern hemisphere autumn). This allows us to explore the effects on the vortex and DD activity caused by the combination of seasonal variations and changes in the properties of the terrain traversed by Perseverance. In addition, we study the effect on vortices and DDs of a regional dust storm that covered Jezero on Ls=153-156° (Mars 2020 sols 312-318),

which significantly affected the local environment (Lemmon et al., 2022). Further insights can be gained through comparisons with models of vortices, simulations of the convective activity at Jezero and an statistical analysis of the closest DD approaches to Perseverance resulting in estimates of the density of DDs in Jezero.

The structure of this paper is as follows. Section 2 describes MEDA datasets and the analyses conducted to identify vortices and dust devils, the results of which are shown in Section 3. Section 4 describes the variability of this activity, including its seasonal evolution, variations associated with the dust storm, and effects linked to different terrains. Section 5 presents a more detailed analysis of a subset of DDs obtained by fitting the observed pressure and winds to a model of a drifting vortex. Section 6 explores a comparison of our in situ data with a Large Eddy Simulation (LES) of vortex activity at Jezero. Section 7 discusses the density of DDs in Jezero and gives details of two DDs that partially damaged MEDA wind sensors. Section 8 presents a summary of our conclusions. Times in this paper are given in terms of Local True Solar Time (LTST).

2 Data and data analysis

MEDA acquires data in measurements sessions that can extend from 5 min. to a few hours and that typically cover 54% of a sol. The data is obtained with a cadence of 1 Hz in most sensors (including pressure), and up to 2 Hz in the 5 Atmospheric Temperature Sensors (ATS) and the two Wind Sensors (WS). Gaps in the data are due to a combination of minor hardware issues and mission operations. The Wind Sensors (WS) were required to be off during orbiter communication passes, and as a result, some observed vortex encounters do not have simultaneous wind data. In addition, one of the two wind sensors was partially damaged on sol 313 by a DD that will be described in Section 7. Wind data obtained afterwards requires modified wind retrievals not yet available at the time of writing this paper. Supplementary Fig. S1 shows the cadence of MEDA observations. About 64% of all vortices detected in the pressure field have simultaneous wind data.

2.1 Vortex detection

We search the entire pressure dataset for vortex pressure drops by using a moving window of a fixed time duration. We use a linear fit to the first and last 10% of the pressure signal disregarding the central 80%. The pressure minus the linear fit form a signal detrended from the daily variation of pressure. When the central point of the detrended signal is at least -0.3 Pa we identify a candidate vortex event and plot the pressure for the event together with a Gaussian and Lorentzian fit to quantify the duration of the event (Ellehoj et al., 2010). The moving window advances by 1 s on each evaluation. We perform several searches of the data with time windows of 80 and 180 s with a detection threshold of 0.3 Pa and searches with a time window of 60, 120, 180, 300, 600 and 900 s with a detection threshold of 0.5 Pa. This dual strategy is based on both the sensor noise level (~ 0.04 Pa, see Sánchez-Lavega et al., 2022) and experiments with the data. Detection thresholds from 0.3-0.5 Pa with long time windows produce numerous false detections caused by small-scale fluctuations of pressure. However, there are many short-duration vortices with pressure dips in the 0.3-0.5 Pa range. Supplementary Fig. S2 shows the cumulative distribution in terms of Δp of pressure drops with a shape characteristic of the passage of a vortex. Power law fits to this distribution have similar slopes for different ranges of Δp , which is a good indication that the survey is complete for pressure dips larger than 0.5 Pa.

Fig. 1 shows examples of typical vortices found on a single sol, and demonstrates how different time windows are needed to identify and quantify the properties of very different events. Fitting a vortex with a Gaussian function or a Lorentzian results in

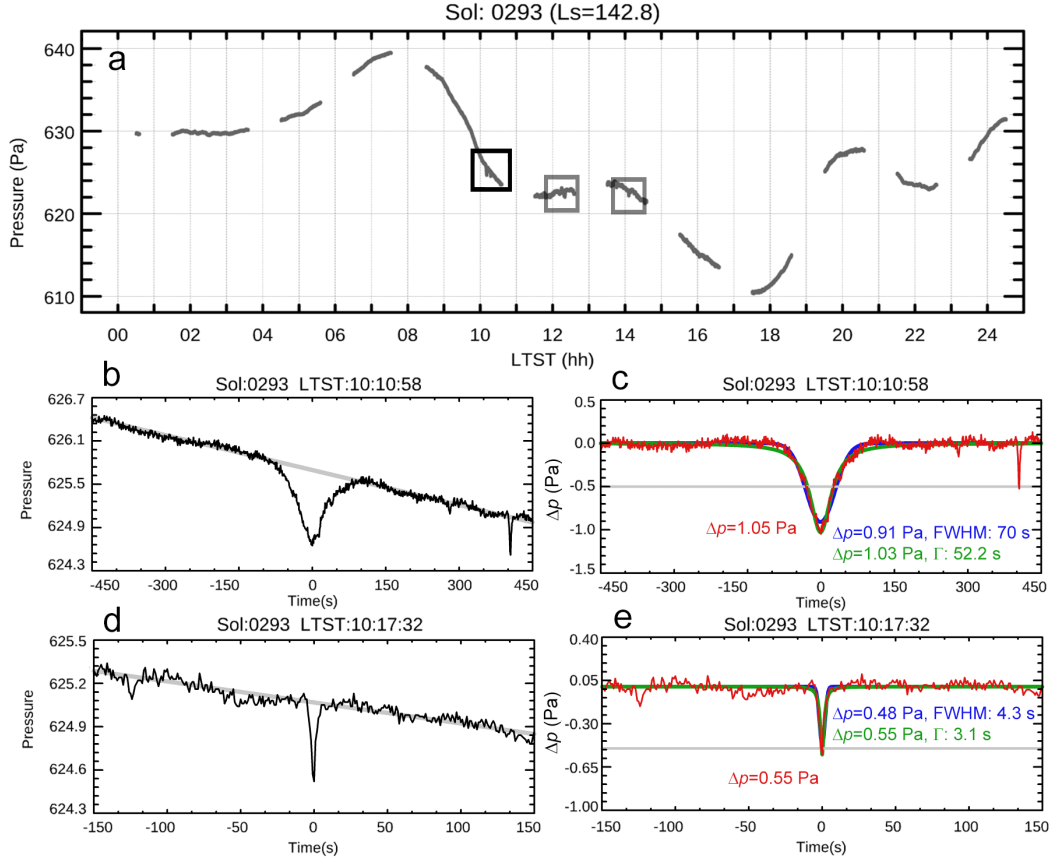


Figure 1. Finding vortices in MEDA data. (a) Pressure over sol 293. Boxes identify the location of four vortices. (b) Two typical vortices. The second one is invisible to the algorithm operating over long time windows. (c) Vortex fitting for the first event in panel (b). Detrended data (red) compared with a Gaussian fit (blue) and a Lorentzian function (green) with similar parameters defining each fit. (d) Second vortex identified using a short time window. (e) Vortex fitting for the event in panel (d).

slightly different values of the intensity of the pressure drop and its duration. Typically these parameters can vary up to 12% in Δp , and up to 25% in the duration of the event. Lorentzian functions generally fit better the central part of the encounter, while Gaussians can fit better the approach and distance phases. Vortices not moving with a constant velocity produce more complex patterns not well fit by these functions (Lorenz, 2013).

Each evaluation of the algorithm generates a catalog of events and a series of plots that are visually examined to remove spurious and duplicate detections and select the time window that results in the best fit to each event. The 300 s time window is found to capture the majority of events, but shorter time windows provide better fits to short or weak events, and long time windows can be required in some cases for a good fit to the data. The longest time windows also allow the detection of longer pressure drops that do not fit a vortex signature, but are instead possibly related to the passage of the low-pressure edges of convective cells. An event of this type is the gust wind event on sol 117 described by Newman et al. (2022) that was associated with a large dust lifting event.

2.2 Vortex characterization

For each event we generate plots of all MEDA sensors using a time window of 8 minutes. These plots are examined to quantify the properties of each pressure drop, such as the simultaneous detection of a change in airborne dust from RDS Top 7. We also examine changes in wind speed and direction, and the thermal response of the surface and the atmosphere to the passage of the vortex. Variations in the lateral RDS detectors can be found both during and outside of the pressure drops, and are caused by vortices passing at a range of distances from very close to the rover up to 1 km. Vortices found in the RDS lateral detectors are not examined in this work and are the subject of a parallel analysis (Toledo et al., 2022).

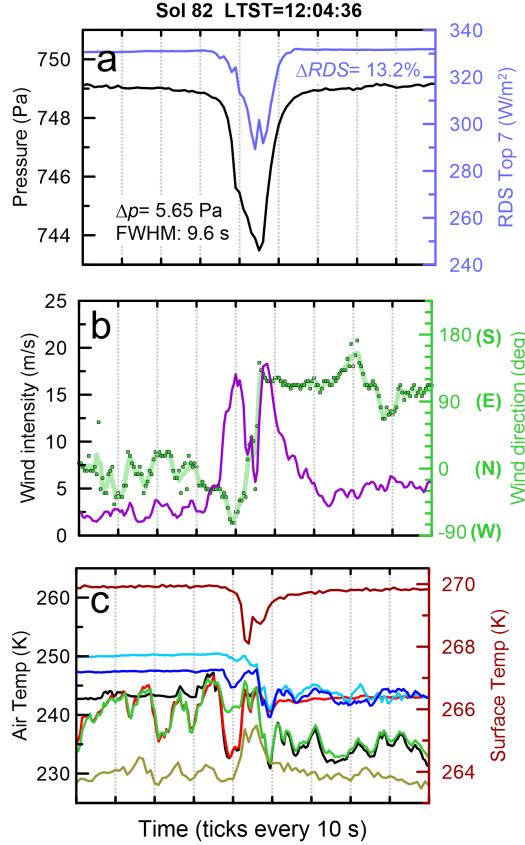


Figure 2. Dust Devil on sol 82. (a) Pressure (black line, left axis) and solar irradiance from RDS Top 7 (blue line, right axis). (b) Wind speeds (purple line, left axis) and direction from which the wind is coming (green line and symbols, right axis). (c) Temperatures during the vortex passage. From top to bottom: Surface temperature (dark-red, right axis); air temperature at $z=0.85 \text{ m}$ from ATS5 (cyan) and ATS4 (dark blue), located at the front of the rover; air temperature at $z=1.45 \text{ m}$ from ATS1 (black), ATS2 (red) and ATS3 (green) located around the Remote Sensing Mast; air temperature at $z \sim 40 \text{ m}$ (green-yellow) from TIRS channel 2. Note the strong thermal gradient of 40 K from the surface to 40 m during this event and the change in wind direction and thermal behavior of the different ATS after the vortex passage.

Fig. 2 shows an example of the multi-sensorial response of the atmosphere to the passage of a strong convective DD. The vortex produced a pressure drop of 5.7 Pa with a Full Width at Half Maximum (FWHM) duration of 9.6 s from the gaussian fit.

The dust in this event resulted in a decrease of the RDS Top 7 signal of 13%, with additional counterparts in RDS lateral sensors (not shown here). This corresponds to an increase of the optical depth of $\Delta\tau = 0.14$, which can be compared with values of optical depths at Jezero over that period of 0.4-0.5 (Rodriguez-Manfredi et al., 2022). MEDA measured winds of 18 ms^{-1} distributed in two peaks coincident in time with half the maximum pressure drop. This symmetric double peak wind structure and its timing with respect to the pressure drop indicate a direct encounter with a vortex, in which each peak in the winds corresponds to the maximum winds in the "walls" of the vortex as it approaches and recedes from Perseverance. This is confirmed from fitting the pressure and wind data from this vortex to models of passing vortices in Section 5. The direct encounter implies that at the central time we are measuring the physical properties of the center of the vortex and that vortices and DDs in Jezero are common enough to produce extremely close encounters, an aspect we discuss in Section 7.

Panel 2c focuses on the complex measurements of temperatures during this event. At the time of this event the rover orientation and ambient wind direction were such that air warmed by the Perseverance's Radio-isotope Thermoelectric Generator (RTG), situated at the rover's rear, was carried over the ATS, creating an increased level of thermal fluctuations (Munguira et al., 2022). With the vortex arrival, the winds bring air not exposed to the RTG reducing the thermal fluctuations to typical levels during the convective period. Our assessment of the thermal plume associated to the vortex from ATS measurements at $z = 1.45 \text{ m}$ is $+8 \text{ K}$. Thermal effects of the vortex at $z = 0.85 \text{ m}$ cannot be quantified for this event, as both sensors are located in the front of the rover and are sheltered from the wind before and after the vortex arrival. Air temperatures obtained by the TIRS instrument at an approximate altitude of $z \sim 40 \text{ m}$ are not affected by the thermal influence of the RTG and show an increase of temperatures during the vortex passage of $+9 \text{ K}$. The ground-surface temperatures, also measured by TIRS, experiences a short cooling of -1.8 K during the vortex passage followed by a gradual recovery of temperatures. An additional change in albedo during this event consistent with the motion of surface particles by the vortex is discussed in Vicente-Retortillo et al. (2022). This example shows that the measurement of the internal thermal structure of vortices is complex and we leave for future work a thermodynamic characterization of a selection of the best cases. On the other hand, the capability to measure the surface-to-air temperature difference at the time of MEDA vortices is an important piece of information that we will examine in Section 4.

3 Pressure drops: Vortices, dust devils, convective cells and waves

3.1 Catalog of pressure drops

Our survey of pressure drops shows events with varied characteristics. Their classification requires a visual examination of the pressure drops and related environmental variables. Figure 3 shows the temporal distribution of 3,900 pressure drops identified by our algorithm and visually classified based on the pressure curve shape. About 2,330 events are compatible with pressure drops caused by vortices with a pressure drop detection threshold of 0.3 Pa . These events are concentrated in the daytime hours with a peak activity near noon. A small number of events are detected also during the night. There are clear changes in the overall activity of pressure drops over the time period of this study. An interesting change occurred on sols ~ 312 -318, when a regional dust storm arrived and was active over Jezero enhancing dust devil activity (Lemmon et al., 2022). During the dust storm a wealth of wavy features was also observed in the nighttime signals, and a significant amount of night time wavy variations in pressure was observed afterwards (Sánchez-Lavega et al., 2022).

Fig. 4 shows examples of pressure curves associated with different types of events. Besides standard cases (a), vortices can be very short (b), or long (c), intense (d), or

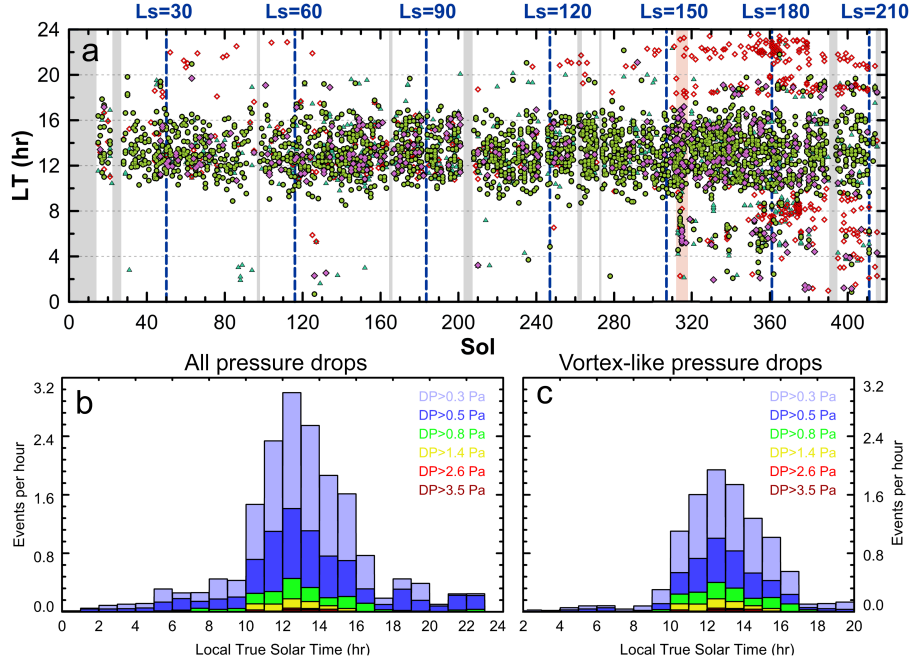


Figure 3. Temporal distribution of pressure drops up to sol 415. (a) Pressure drops as a function of sol/Ls and LTST. Green circles show vortex-like pressure drops with $\Delta p > 0.3$ Pa identified from the shape of the pressure curve. Red diamonds show long and smooth pressure drops compatible with atmospheric waves. Purple diamonds show long pressure drops with strong pressure fluctuations, possibly indicative of turbulent periods. Green triangles show long events with $0.3 \text{ Pa} < \Delta p < 0.5 \text{ Pa}$, similar to smaller amplitude waves or turbulent events. The light orange dashed region highlights a period of time with an active dust storm over Jezero. Grey dashed regions indicate sols without data. (b) Daily distribution of all pressure drops corrected from sampling effects. (c) Daily distribution of pressure drops compatible with vortices corrected from sampling effects.

weak (e), simple (a), or complex in terms of their pressure curves (f-g), including nearly double or very close events (h). Some of the nighttime vortex-like pressure drops are coincident with turbulent pulses of high-temperatures measured with the ATS. These events are most likely caused by weak winds flowing above the rover's RTG (i), and, thus, are similar to the nighttime vortices found by the Viking Lander, which were attributed to the Lander acting as a heat island Ryan & Lucich (1983). MEDA data allows us to demonstrate the artificial nature of some of these events thanks to wind measurements showing the direction of the winds coming from the RTG position at the back of the rover towards the front of Perseverance. Other nighttime pressure dips equivalent in shape to those caused by daytime vortices, are found in the data with winds coming from the opposite direction of the RTG, with no clear thermal counterparts and equivalent to other nighttime pressure drops found in other Martian locations (Ordóñez-Etxeberria et al., 2018; Chatain et al., 2021). A further type of event consists of long and turbulent pressure drops observed near noon, which sometimes exceed durations of 300 s (j-k). Some of these can be interpreted as the passing of convective cells, as a remarkable event found on sol 117 and discussed in (Newman et al., 2022). However, the interpretation of the individual nature of these events requires examining additional data beyond pressure. Finally, pressure drops caused by atmospheric waves are also identified in the general pattern of pressure

284 drops (l). These were particularly abundant after the dust storm on sols 308-316 and
 285 are discussed by Sánchez-Lavega et al. (2022).

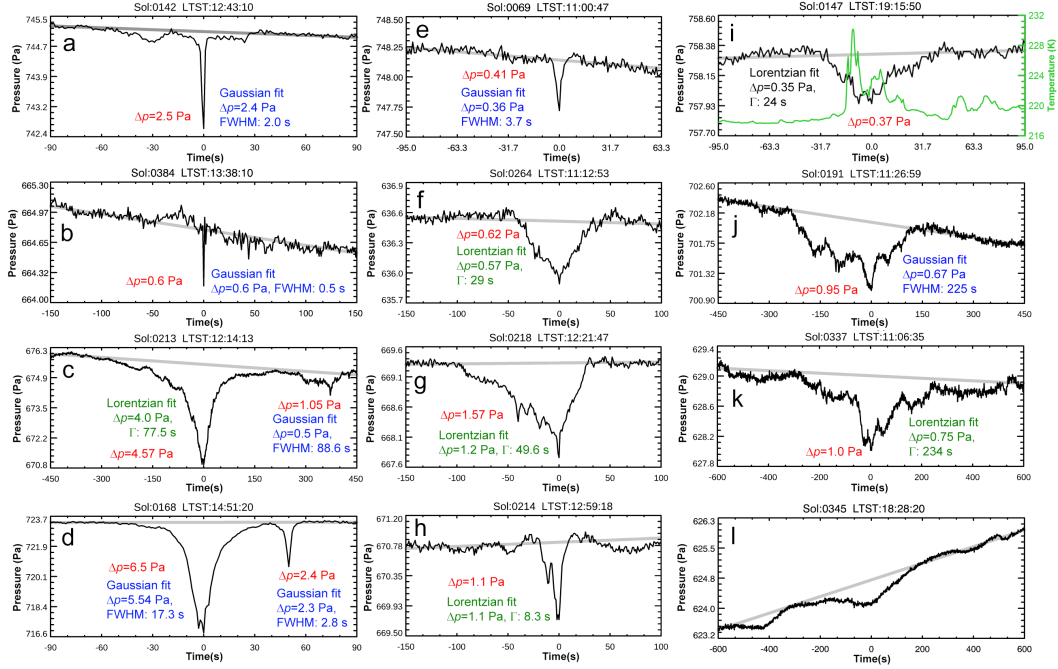


Figure 4. Variety of pressure drops on Jezero. (a-d): Typical vortices. (a) Typical vortex. (b) Shortest event. (c) Long and intense pressure drop followed by a secondary event. (d) A very intense pressure drop with an internal structure followed by a secondary event. (e) Low intensity vortex. (f) Vortex with a wide pressure drop. (g-h) Complex events showing signature of superposition of vortices or complex trajectories. (i) Long pressure drop during the night accompanied by a thermal plume originated over the RTG (right-axis). (j-k) Long and noisy events typical of near-noon hours. (l) Series of wavy structures in the nighttime pressure.

286 The overall pattern of vortices, turbulence and waves at Jezero after the dust
 287 storm period is similar to the northern autumn activity described at the Insight landing
 288 site by Chatain et al. (2021) with bursts of daytime vortices, nighttime vortices and
 289 intense nighttime turbulence. Future analyses over a full Martian Year will be needed
 290 to asses if this change in activity was caused by the dust storm or seasonal evolution.

3.2 Vortices and Dust Devils

291 We identify DDs as events with a pressure drop of at least 0.3 Pa and a simulta-
 292 neous reduction in irradiance captured by the RDS Top 7 sensor of at least 0.5%
 293 (corresponding to a $\Delta\tau = 0.05$). Figure 5 shows the temporal distribution of vortices
 294 (a; 2,328 events, where 1,058 events have a $\Delta p > 0.5$ Pa) and DDs (b-c; 238 events
 295 with $\Delta RDS \text{ Top } 7 > 0.5\%$). Panel (d) shows that intense vortices with large pressure
 296 drops tend to be dusty. Only 1.8% of the vortices with a pressure dip from 0.3 to 0.5
 297 Pa had a simultaneous detection of dust. About 20% of all pressure drops with ΔP
 298 > 0.5 Pa have dust and this fraction increases for higher values of the pressure drop
 299 becoming 66% for events with $\Delta P > 2.0$ Pa and 100% for events with $\Delta P > 4.3$ Pa
 300 (Supplementary Fig. S3). Panel (e) shows that the duration of vortices containing
 301 dust tends to be smaller than non-dusty vortices implying smaller diameters for dust
 302

devils events. However, a few extremely long DDs with FWHM of up to 220 s are also found. Supplementary Fig. S4 details the distributions of FWHM of the population of vortices and DDs.

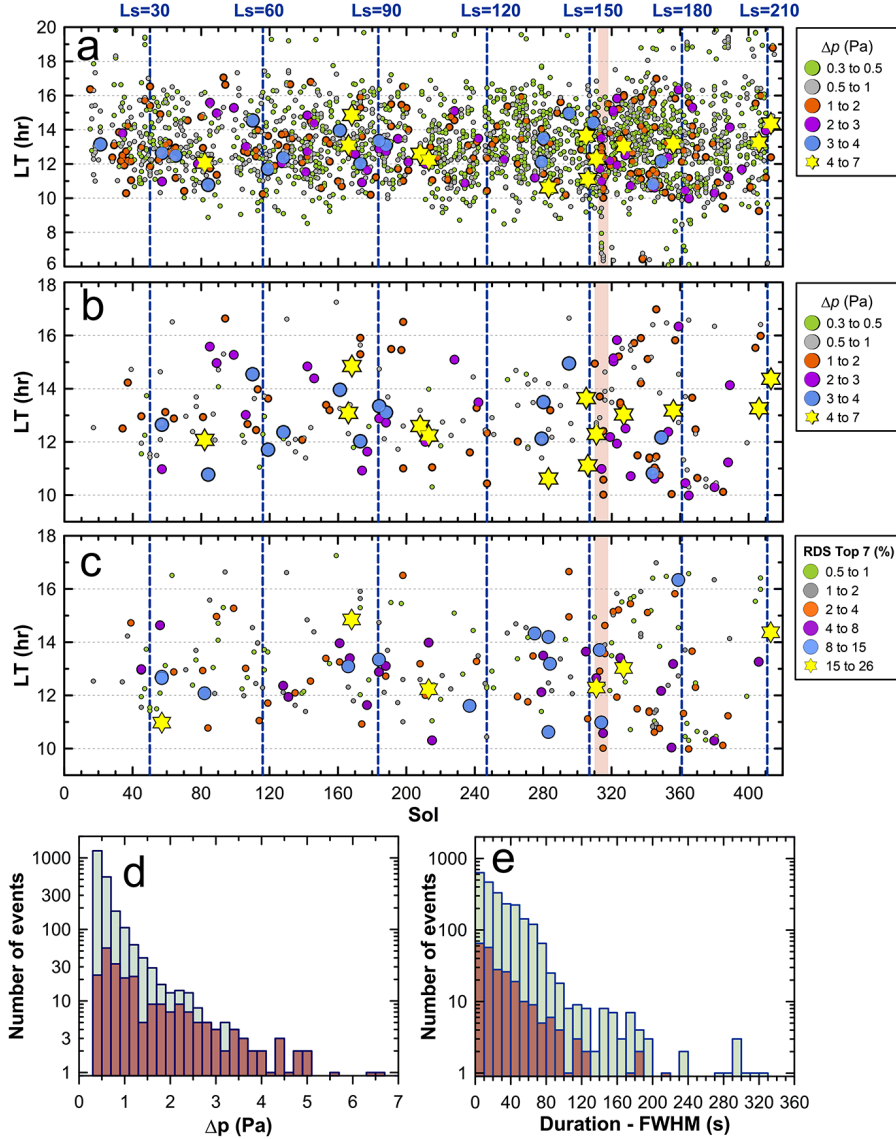


Figure 5. Distribution of vortices and dust devils. (a) Temporal distribution of vortices. Symbols identify events of different intensities. (b) Same as (a) but only for events with a RDS Top 7 detection of a dip in irradiance of at least 0.5%. (c) Same as (b) but showing here the level of dustiness of individual DDs. (d) Histogram of the number of events with a given pressure drop. (e) Histogram of the number of events with a given duration. Light-green bars in (d) and (e) correspond to all vortices and dark brown bars correspond to DDs. The period of the dust storm is highlighted with a shaded region in panels (a-c).

We explore the relationship between the intensity of the pressure drop detected, its duration, and observed dustiness in Figure 6. These aspects depend on a combination of distance to closest approach, vortex diameter, dust density in the DD, and solar illumination. Events with pressure drops higher than 2.0 Pa are typically

short ($\langle \text{FWHM} \rangle = 26$ s, with maximum FWHM of 160 s) and dusty. They probably represent relatively close encounters with DDs. Dusty events with pressure drops smaller than 1.0 Pa are more numerous and tend to be longer ($\langle \text{FWHM} \rangle = 41$ s and maximum FWHM of 215 s). They probably represent the more distant passage of vortices intense enough to raise dust. The very few DDs with pressure drops smaller than 0.5 Pa have $\langle \text{FWHM} \rangle = 20$ s and might be DDs in the process of losing strength and vanishing, rather than detections of distant vortices carrying dust. Panel c in this figure also shows the distribution of dust devils per hour corrected for the uneven temporal sampling with MEDA and can be directly compared with Fig. 3c for the vortex activity.

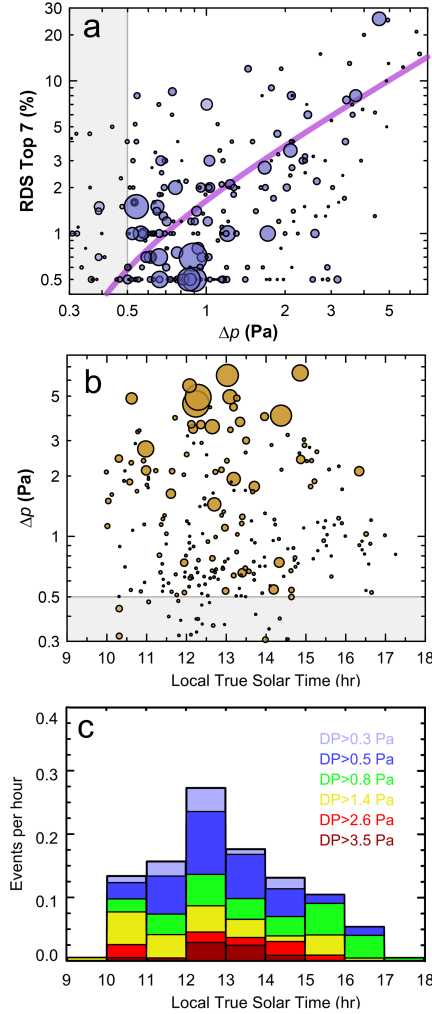


Figure 6. DDs pressure intensity, duration and dustiness. (a) RDS Top 7 decrease as a function of Δp . The circle size identifies the duration of each event from 1.0 (smallest) to 200.0 s (largest). The purple line is a fit to the data with a squared coefficient of regression $r^2=0.40$ (40% of the variations of the irradiance decrease is directly related to the variations in Δp). (b) Daily distribution of dust devils. The circle size codifies the reduction of irradiance detected from 0.5% ($\Delta\tau=0.05$) to 26 % ($\Delta\tau=0.30$). (c) Histogram of the number of dust devils events per hour corrected from sampling effects associated to different sampling at different hours. The characteristics of the data make the survey incomplete for events from 0.3 to 0.5 Pa.

4 Variability of vortex and dust devil activity

Perseverance moved about 10 km as the seasons evolved from early Spring to Autumn over the first 415 sols of the mission. Several changes in the vortex and dust devil activity were observed in this period. Because events with pressure drops smaller than 0.5 Pa are more difficult to characterize and only represent a tiny fraction of the DDs detected, we only explore seasonal variability for events with $\Delta p > 0.5$ Pa.

4.1 Seasonal evolution

Figure 7 displays histograms of the daily activity of vortices corrected from sampling effects in four different periods. Numerical models predicted that the most intense daily activity of vortices and dust devils should occur at noon in early Summer around $L_s=120^\circ$ (Newman et al., 2021). The data shows that this is indeed true. However, the vortex and DD activity remained strong after $L_s=120^\circ$ with a more spread-out activity over different hours in that period. The number of dust devils at Jezero detectable by MEDA grew from 0.7 events per sol in early Spring to 1.2 events per sol at the end of the Summer (correcting from gaps in MEDA coverage).

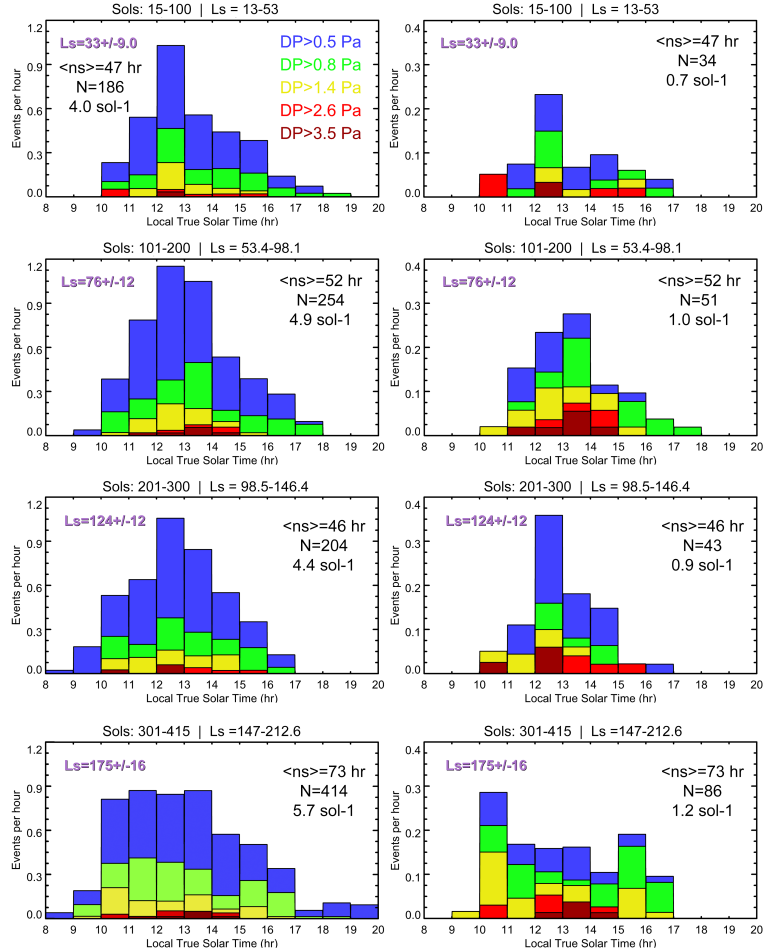


Figure 7. Daily histograms of vortices (left column) and DDs (right column) over different periods. All histograms are corrected from sampling effects and observational gaps. The figure also shows the average number of hours observed each LTST, n_s , the total number of events detected, N , and the mean number of events produced per sol in each period.

Maximum irradiation at the top of the atmosphere occurred at the latitude of Jezero on sol 337 ($L_s=166^\circ$). This was a period characterized by higher atmospheric opacity and weaker surface-to-air temperature gradient than earlier in the mission with a relatively low vortex activity. The maximum surface temperature at Jezero, and maximum near surface thermal gradient, was found around sol 280 ($L_s=136^\circ$) (Munguira et al., 2022), which agrees with the cluster of strong DDs found on sols 280-330 including the period covered by the dust storm. This is in agreement with the correlation found by Spiga et al. (2021) between the number of diurnal vortices and the sensible heat flux from the surface to the atmosphere from Insight data.

4.2 Dust Devil Activity during the $L_s=153^\circ$ Dust Storm

A regional dust storm passed over Jezero from sols 312 to 318 ($L_s=152.8-156^\circ$). The storm brought significant changes in atmospheric opacity (Lemmon et al., 2022), temperatures (Munguira et al., 2022), and behavior of pressure (Sánchez-Lavega et al., 2022), and also mobilized large amounts of dust and sand that caused a decrease in surface albedo (Vicente-Retortillo et al., 2022). Lemmon et al. (2022) present a detailed study of the dust storm. Dust Devil Surveys and Dust Devil Movies that were obtained during the dust storm observed a record number of 14 dust devils on sol 313 over 11:35-11:59. One of the MEDA wind sensors was partially damaged during one DD approach on sol 313 (see Section 7).

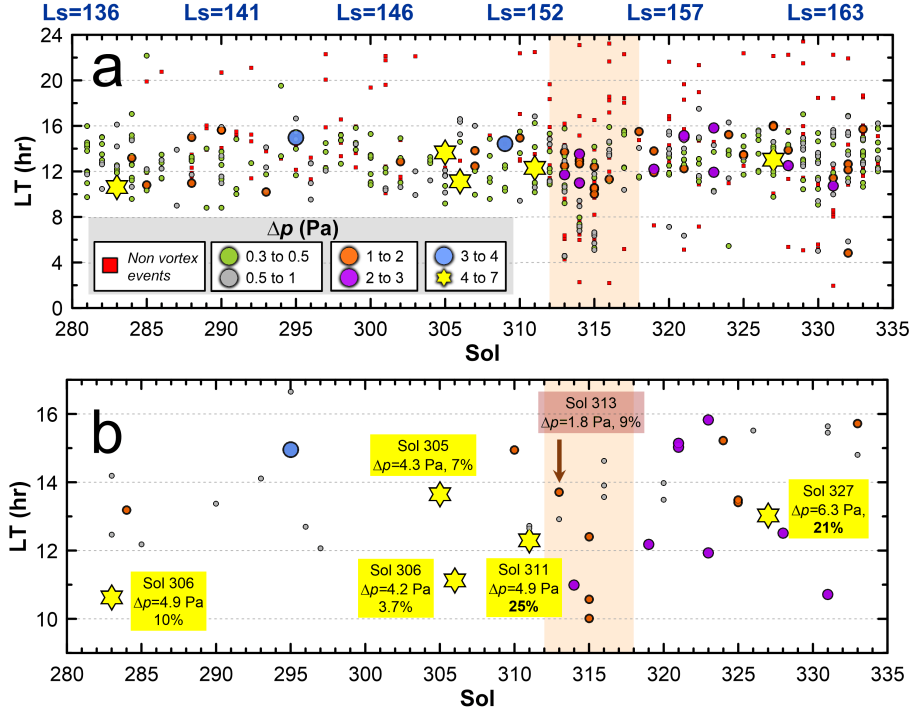


Figure 8. Vortex and dust devil activity during the dust storm. (a) All pressure drops from sols 280 to 335. (b) Dust devils in the same period. Red squares in (a) correspond to pressure drops not caused by vortices. Symbols identify the intensity of the pressure drop. Shaded areas highlight the period of dust storm over Jezero. The intensity Δp of individual events and percentages of the reduction of light measured by RDS are given in (b) for selected events. A DD highlighted with an arrow in (b) damaged part of the hardware of one wind sensor on sol 313 at 13:38. LTST.

MEDA detections of vortices and DDs around and during the dust storm period are presented in Fig. 8, which shows that vortex and DD activity picked up several sols before the storm reached Jezero. The largest concentration of vortex detections occurred over sols 313-315, but most of them were weak in terms of their Δp . These sols were those with the higher dust opacity in the atmosphere and were accompanied by a reduction in the surface to air thermal gradient caused by air temperatures that increased +14 K compared with previous sols (Munguira et al., 2022). Pressure oscillations not related to vortex activity started to be numerous around sol 313 and changed the pattern of small nighttime pressure oscillations after the dust storm died away (Sánchez-Lavega et al., 2022). Although the sampling cadence over this period was higher than in previous sols (Supplementary Fig. S1), the increase in DD detections is significant. DDs in Figure 8b show a concentration of 1.5 events detected per sol that translates in 2.0 events per sol if we correct from the time sampling over sols 310-318, which doubles the inferred activity of 1.0 events per sol for that seasonal period. There were no events detected on the last few sols of the storm (317-318), which also corresponded to lower surface and air temperatures and reduced surface to air thermal gradient (Munguira et al., 2022). The recovery to normal environmental conditions occurred in sol 318, when the dust opacity (Lemmon et al., 2022), pressure (Sánchez-Lavega et al., 2022) and temperatures (Munguira et al., 2022) returned to normal levels.

The dust devil activity during the dust storm was very different to that observed by Curiosity at Gale crater during the MY34/2018 Global Dust Storm (GDS) (Guzewich et al., 2019), when a strong suppression of vortex activity was observed for most of the storm (Ordóñez-Etxeberria et al., 2020). This suppressed vortex activity occurred when the dust opacity grew to $\tau = 3.5$, and vortex activity recovered when the dust opacity diminished to $\tau = 1.5$. The situation at Jezero was more similar to that observed by Insight during a Large Dust Storm (LDS) on 2019 (Viúdez-Moreiras et al., 2020). The MY34/2019 LDS developed at $L_s=320^\circ$, reaching peak values of $\tau = 1.9$ with a temporal duration of ~ 110 sols. Insight observed an enhancement of vortex activity during the storm onset, and a reduction in its long decaying phase. In the 2022 dust storm at Jezero, there was a cluster of intense events before the storm, an increase of activity over sols 313-315 with a dust opacity peak of $\tau = 2.4$ on sol 314, and a reduction of activity over the decaying phase of the dust storm that extended only until sol 318, when τ was down to 1.3 (Lemmon et al., 2022). This phenomenology represents a faster version of what was observed by Insight during the longer-lived 2019 LDS.

4.3 Variations of DD activity correlated with terrain properties

There are fundamental differences between meteorological stations fixed in a landing site (Viking Landers, Phoenix and Insight) and those in moving rovers (Mars Exploration Rovers, Curiosity, Zhurong, and Perseverance) that sample atmospheric properties over different terrains. An important result from MEDA is the small-scale spatial distribution of Thermal Inertia (TI) of the terrain, which is measured from a combination of TIRS and RDS data (Rodríguez-Manfredi et al., 2022; Martínez et al., 2022). MEDA derived values of TI range from 180 to 610 $Jm^{-3}K^{-1}s^{-1/2}$ (TI units hereafter). These values are comparable to values obtained from orbit by the THEMIS instrument (Fergason et al., 2006) on the Mars Odyssey orbiter. THEMIS data in the Jezero region has a spatial resolution of $\sim 100 \times 100 m^2$, and average values of Thermal Inertia of ~ 300 TI units for Jezero. MEDA measures values of TI over small patches of the terrain observed in the FOV of TIRS, which covers an area of $3 m^2$. These measurements show strong variations in the values of TI over the rover's traverse that correlate with strong variations in the vertical thermal gradient of the atmospheric surface layer (Rodríguez-Manfredi et al., 2022; Munguira et al., 2022). The vertical thermal gradient of the atmospheric surface layer is a

key element in producing convective vortices, and more frequent and more intense vortices are expected over low TI terrains that favor higher vertical thermal gradients of temperature (Rennó et al., 1998; Spiga et al., 2021). Figure 9 shows a map of Jezero’s TI from THEMIS data with the rover’s trajectory and the DDs detected. We show the intensity of the pressure drop of individual events and the decrease of light measured by RDS on the dustiest DDs. These are compared with the derived values of thermal inertia from MEDA up to sol 380 (later sols correspond to frequent drives during a rapid traverse phase that did not allow to measure TI).

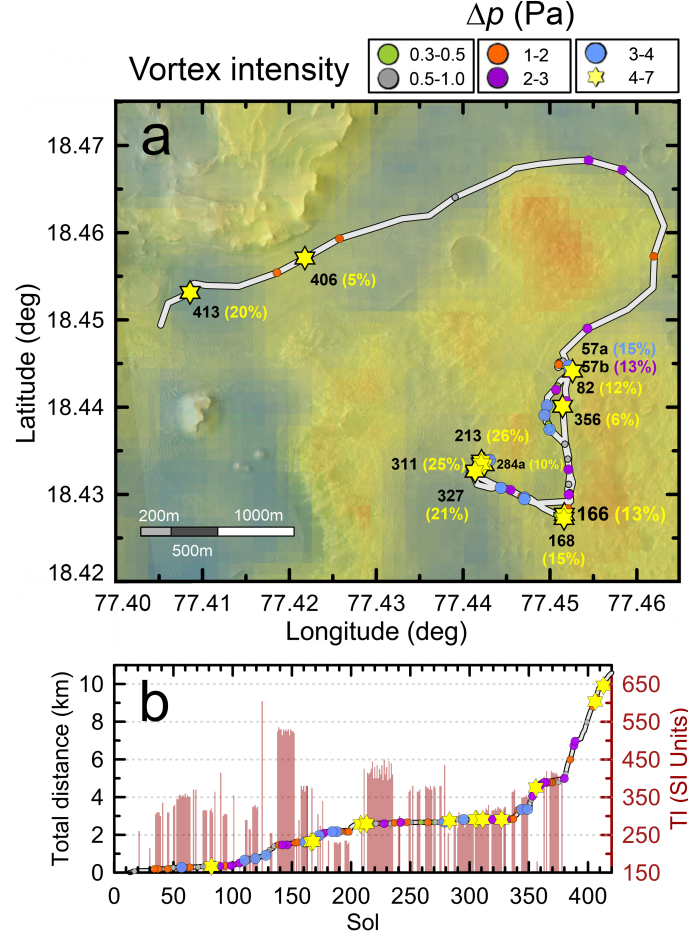


Figure 9. DDs over Perseverance’s traverse. (a) THEMIS map of thermal inertia, rover trajectory (line) and DDs identified with symbols quantifying the intensity, Δp of the pressure drop. Black numbers correspond to sols with the most intense events. Colored numbers give the percentage of light decrease in RDS Top 7. (b) Distance travelled by Perseverance (grey line, left axis) compared with thermal inertia of the terrain (vertical bars, right axis) with individual events superimposed following the same symbols as in (a).

Figure 10 shows relations between vortex properties, the vertical thermal gradient of the atmosphere from the difference between the surface temperature and the air temperature at 40 m and the TI of the terrain. The vertical thermal gradient is calculated for a time window of 8 minutes around the vortex passage, and is a function of LTST and surface TI with only minor effects from seasonal changes. The daily distribution of vortices as a function of the vertical thermal gradient shows that local

terrains with values of thermal inertia larger than 400 TI rarely produce vertical thermal gradients at noon larger than 25 K, and the associated vortices are less intense and have a lower probability to become DDs. We note that the distribution of DDs follows the same trend as that of the intense vortices.

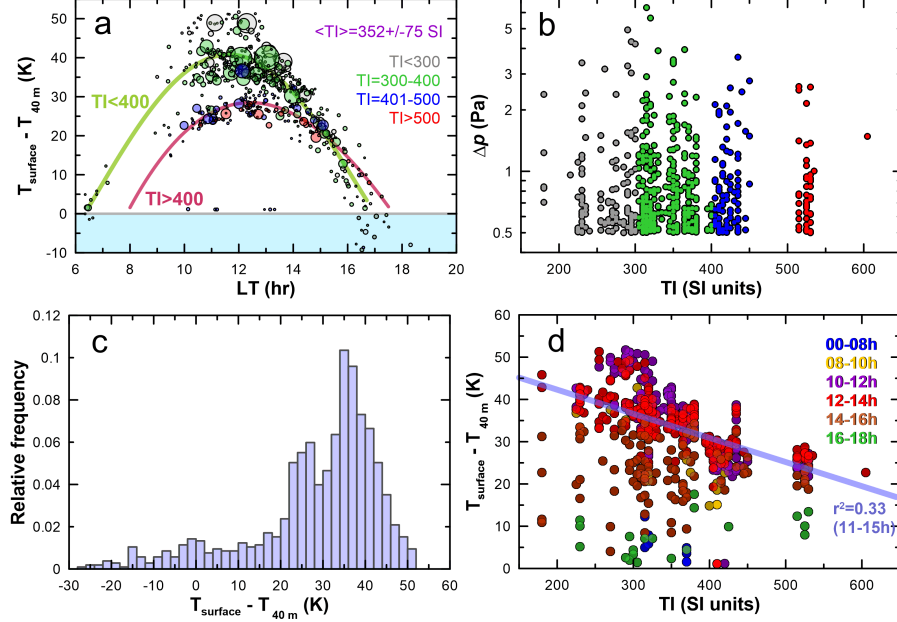


Figure 10. Vortices intensities in terms of their Δp , vertical thermal gradient of the atmosphere, and surface thermal inertia. (a) Distribution of vortices as a function of LTST and the vertical thermal gradient. Individual vortices are plotted with circles whose size indicates the intensity of Δp from 0.5 (smallest) to 6.5 Pa (largest). Colors correspond to different values of the surface TI. Polynomial fits to vortices found over terrains with TI < 400 and TI > 400 are shown with green and red lines respectively. The r^2 coefficient of determination of the fits are 0.84 and 0.62 in the green and purple lines respectively. (b) Scatter plot of the intensity of pressure drops for all vortices compared with the values of the local TI. Colors correspond to those used in panel (a). (c) Histogram of the number of vortices found for different values of the vertical thermal gradient. (d) Relation between the surface TI and the vertical thermal gradient. Circles identify different vortices and colors their LTST. A linear fit to data close to noon hours is shown with a blue line.

Supplementary Fig. S5 shows a scatter plot of pressure drops of DDs and the vertical thermal gradient during these events showing also their observed dustiness from the RDS Top 7 decrease of irradiance. The most intense events are not always found for the strongest vertical thermal gradient, but a temperature difference of at least 20 K between the surface and the atmosphere at ~ 40 m is needed to form intense vortices and DDs.

5 Physical properties of Dust Devils from model fitting

Our vortex and dust devil observations are sensitive to a combination of the physical properties of the vortex and the geometry of its encounter with the rover. In order to obtain realistic values of the physical parameters of DDs we compare pressure and wind data of MEDA vortices with a model of a drifting vortex (Lorenz, 2016)

Vortex parameters

Δp_0	Pressure drop at the vortex center
D	Diameter of the vortex (maximum winds)
S	Vorticity sign: Positive for counter-clockwise rotation, negative for clockwise
α	Cyclostrophic factor from 0.5 (fully cyclostrophic) to 1.0

Geometrical and environment parameters

d_{min}	Minimum distance
$Path :$	(+) for vortices at y positive when closest (-) for vortices at y negative when closest
U	Vortex drift velocity
Ω	Vortex drift direction angle (measured clockwise from the North)

Table 1. Parameters defining a vortex encounter.

following a similar approach to (Kahanpää & Viúdez-Moreiras, 2021) without fitting the RDS signals. We calculate the pressure drop at the center of the vortex, ΔP_0 , and its diameter D , together with the trajectory of the vortex and its minimum distance to Perseverance.

5.1 Methodology

We assume vortices that move in a straight line with the environment winds. The parameters that define the pressure and winds at a fixed location are given in Table 1. We also assume a Lorentzian pressure drop and vortices close to cyclostrophic equilibrium that follow:

$$V_t = \sqrt{\alpha \Delta p_0 / \rho}, \quad (1)$$

where V_t is the maximum tangential velocity of the vortex at the vortex edge, Δp_0 is the pressure drop at the vortex center with respect to the environment, ρ is the atmospheric density, and α is a free parameter from 0.5 to 1.0 that allows deviations from cyclostrophy, with 0.5 representing a fully cyclostrophic vortex (see discussion in Kurgansky et al., 2016).

We implement the numerical model from Lorenz (2016) and follow a Monte-Carlo approach to find the parameters that best fit MEDA pressure and wind data for selected vortex encounters. For each vortex we generate random values of the parameters in Table 1 within reasonable ranges for each parameter, and compare the modelled pressure and winds with MEDA observations. Because we are sampling a 6-dimensional space of parameters (plus the uncertainty in vortex rotation and path) we test $\sim 20,000$ to $50,000$ models for each of the MEDA vortices analyzed. We calculate values of χ^2 for pressure and wind and we use a combined figure of merit χ^2 to select the best fits. The parameters of models that best approach the observations of a MEDA vortex converge in narrow ranges. To refine the fits, we launch a second set of $20,000$ - $50,000$ models in the parameter region that contains the best models. The parameters that best reproduce the observations are defined with the statistics of the ten best models, which are visually examined to confirm they represent a close match to the observations. Supplementary Figure S6 shows an example of the procedure for the strong DD observed on sol 82 (see Figure 2).

For the DD on sol 82, Figure 11 shows a comparison of the three best models and the MEDA data. The parameters that fit the DD on sol 82 correspond to a vortex with a diameter of 11.4 ± 4.0 m passing at a closest approach of MEDA of 0.0 - 0.4 m with a mean crossing distance of 0.15 m and anticlockwise rotation. Such a close

approach implies a central pressure drop of 5.6 ± 0.3 Pa essentially identical to the one observed by MEDA. Because of the stronger variations in winds than in pressure crossing distances are more representative of the distance to the rover wind sensors than to the pressure sensor.

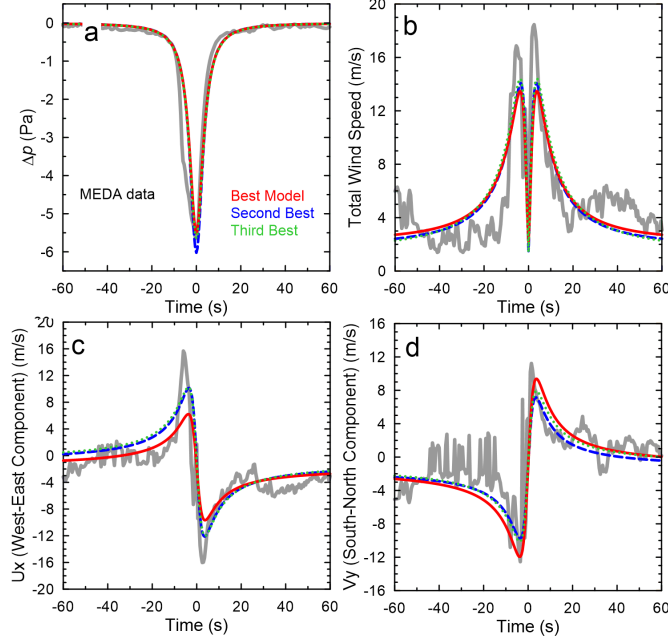


Figure 11. Comparison of MEDA data and best models for the Dust Devil on sol 82. (a) Pressure. (b) Total wind speed. (c) Zonal (west to east) component of the wind. (d) Meridional (south to north) component of the wind. Grey lines show MEDA data. Colored lines show the best three models.

This method has been validated for a DD on sol 215 also imaged by Navcam and observed acoustically by the SuperCam Microphone (Murdoch et al., 2022). Vortex properties were obtained independently from Monte-Carlo modeling of the MEDA data, from the acoustic data, and from images, and were found to be highly consistent with each other.

5.2 Results

There are 131 DDs with wind data in the MEDA data presented here. We selected 22 events that we analyzed individually. These DDs were the most intense, more dusty, and those with a strongest wind signature. This implies a strong bias towards close encounters with DDs. An event specifically selected to explore this bias is the DD on sol 264, whose pressure curve is shown in Figure 4f and has a wide central pressure drop that could be considered as representative of a distant vortex. This event was accompanied by a weak reduction of irradiance in the RDS Top 7 with longer signals in the RDS Lat detectors.

Our results for the sample of 22 vortices result in values of $\alpha = 0.65 \pm 0.08$ with 40% of the vortices having clockwise rotation and 60% having anti-clockwise rotation, which implies an equal distribution of the sense of rotation. Figure 12 shows the results for our fits to DDs. These DDs have central pressure drops comparable or up to twice the observed Δp in MEDA data. Most events have crossing distances smaller than

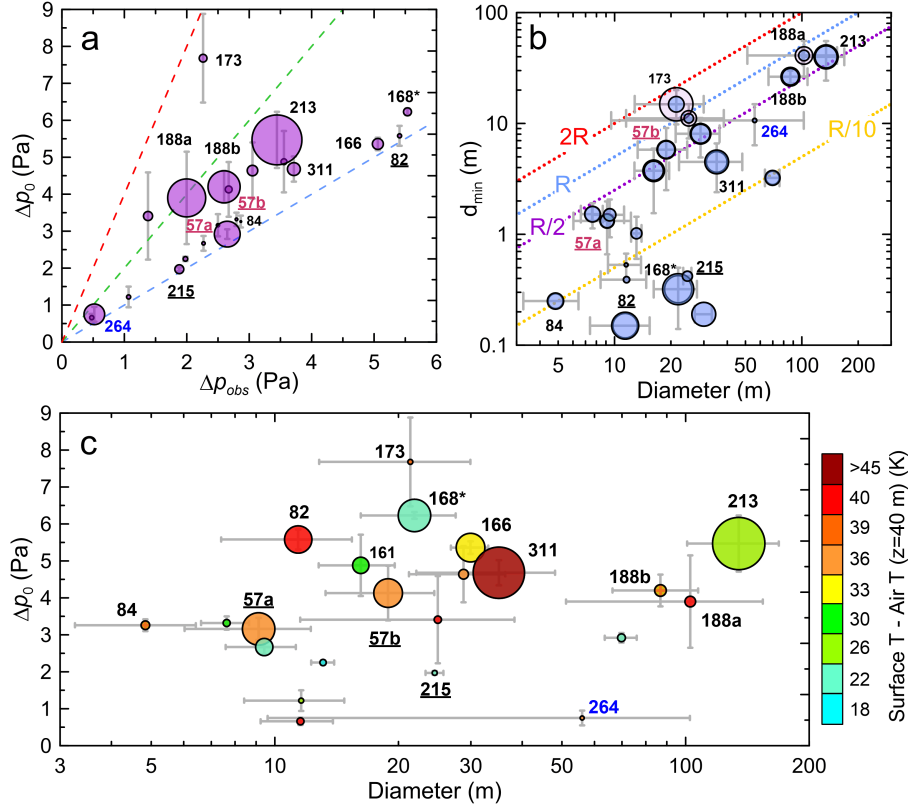


Figure 12. DDs from modeling pressure and winds. (a) Δp_0 at the vortex center as a function of the observed Δp_{obs} . Circle sizes represent vortex diameters from 4.8 to 135 m. Dashed lines correspond to $\Delta p_0 = n\Delta p_{obs}$ with $n=1, 2, 3$ (blue, red, green respectively). (b) Minimum distances compared to vortex diameters. Circle sizes indicates the observed pressure drop (inner circle) and at the vortex center (outer circles). Diagonal dotted lines show crossing distances as a function of the vortex radius R . (c) Scatter plot of vortex central pressure drop and vortex diameter. Circle sizes indicates irradiance decrease in the RDS Top 7 from 0.5 % to 26%. Numbers indicate sols of specific events. Underlined events have been specifically modelled here or in Vicente-Retortillo et al. (2022); Murdoch et al. (2022). Colors indicate the thermal gradient of the atmospheric surface layer ($T_{ground} - T_{air}$ at $z \sim 40$ m) for each event.

the vortex radius and only a few events are observed at a distance comparable to the vortex diameter. For the DD on sol 264 that was selected to test distant passages we find that while our model simulations converge towards a close encounter, there very large error bars associated to the small pressure perturbation and weak winds observed during this event.

The vortices have diameters from 4.8 to 135 m, the latter found in the event in sol 213 at 12:14 LTST. This DD was discussed by Newman et al. (2022), as it was a dusty event with a reduction in the RDS Top 7 irradiance of 26% ($\Delta\tau = 0.3$, the largest in 415 sols). This large opacity can be explained by a dusty vortex with a diameter of 135 m crossing at a minimum distance of 40 m from Perseverance. Paradoxically, this intense and large event occurred under a small vertical thermal gradient over a terrain with a relatively high local surface thermal inertia of 420 SI units. However, this was a large vortex that may have formed over nearby terrains with a more typical vertical thermal gradient.

We note that the estimation of the size scale of this event given in Newman et al. (2022) was 300 m, estimated as the distance traversed during the FWHM of the event at the environment wind speed u . Here we find a smaller diameter of 135 m from our fits to models of this event. We interpret the distance obtained in Newman et al. (2022) as the distance traveled by the vortex while its properties can be sensed by MEDA. Given its minimum crossing distance (40m) and size (68m in radius), the vortex was detected at distances of 150 m, or 2.3 times its radius. For most of the vortices that we have modeled, we find that the estimated diameters given in Newman et al. (2022) should be corrected by dividing by 3.

Another interesting DD is the event on sol 173 at 12:01 LTST. This was a 3.2 Pa pressure drop with a temporal duration of 45 s. The vortex was accompanied by variations in the winds of 20 ms^{-1} and a small reduction of irradiance at the RDS Top 7 sensor (0.5%, $\Delta\tau=0.05$). The parameters that fit this event converge in a vortex with a diameter of 12-30 m crossing at a distance of 10-20 m. This intense vortex may have had a central pressure drop of 6.5-9.0 Pa. This upper limit is similar to the most intense vortices directly detected at Elysium Planitia by Insight (Spiga et al., 2021).

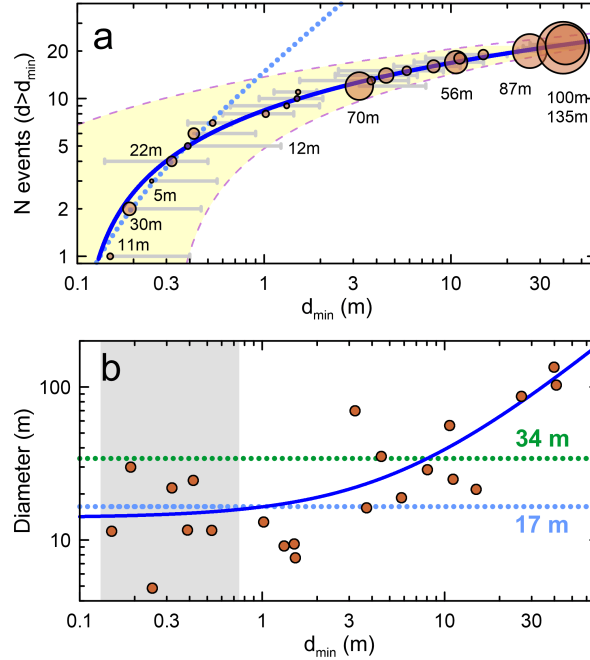


Figure 13. Crossing distances and diameters of DDs. (a) Cumulative distribution of DDs as a function of their crossing distance. Circles represent individual events with the size of the circle representing vortex diameters from 5 to 135 m. Error bars are calculated from the Monte-Carlo fits to each event. The blue line is a logarithmic fit to all the data. The dotted line is a linear fit to the first 7 events extended to the limits of the plot. (b) Diameter of individual DDs as a function of their crossing distance. Events with a crossing distance smaller than 1 m appear in the shadowed area. The blue solid line shows a linear fit to all the data. The light-blue dotted line shows the average of the 7 closest events suggesting that the most common diameter is 17 m. The green dotted line shows the average of all DDs that have a calculated diameter.

From our model fits to the most intense vortices we have found their likely crossing distances. There are 7 DDs for which the vortex center is modeled to have passed within 1 meter of Perseverance. These vortices are sensed in their true magnitude and

provide an unbiased sample of the properties of vortices at Jezero. Figure 13a shows the vortices whose properties we have been able to fit ordered with respect to their minimum crossing distance. A linear fit to the 7 vortices with closest approaches has an r^2 regression coefficient of 0.986.

We examine the distribution of diameters in Figure 13b. For the very close approaches, representing an unbiased sample, the diameters of the vortices characterized is 17 ± 8 m, which is comparable to the diameters of vortices in images of Jezero shown in Newman et al. (2022). There are three vortices with a diameter of 100 m passing at a distance of 30 m and the mean diameter of all the vortices with model fits is 34 m. Thus, while the average diameter of vortices at Jezero can be constrained to 25 ± 8 m, most DDs at Jezero have diameters of $\sim 17 \pm 8$ m. In addition, the events with crossing distance below 1.0 m have central pressure drops from 0.7 to 5.6 Pa with an average value of 3.5 Pa. This can be considered as a typical central intensity of frequent vortices at Jezero. More intense events, with values of central pressures up to 9.0 Pa appear only rarely, and we have only observed one of them at a large distance resulting in a smaller value of observed Δp .

The distance of approach of the closest passing vortices and the frequency at which we observe the largest vortices constitute a set of strong constraints on the density of dust devils in Jezero and their size distribution, as will be analyzed in Section 7.

6 Comparison with LES results

In order to gain further insight in to the complexities of characterizing a sample of vortices from measurements obtained with a single station, we explore vortices in a LES representative of the conditions at Jezero and analyze the data from the simulation with the same algorithm used for MEDA. We examine one MarsWRF (Richardson et al., 2007) simulation of Jezero crater in LES mode (Wu et al., 2021; Newman et al., 2022). The LES grid has an horizontal resolution of 10 m over a region covering 10x10km with periodic boundary conditions. The model output is given every 10 s. A background wind of 4 m/s, comparable to daytime winds at Jezero, is imposed. The latitude, surface properties (e.g., height, albedo), and dust loading are chosen to match Jezero crater at $L_s \sim 45^\circ$, and the simulation is started at 06:00 LTST and continued through 15:00. Results presented below correspond to half an hour starting at noon.

6.1 Vortices and pressure drops in the LES

The LES shows the presence of intense vortices mixed with convective cells and turbulence. Figure 14a shows a snapshot of the simulation where vortices create local minima of pressure. Figs. 14b and 14c show the tracks of the 20 most intense vortices in each time step of the simulation as they drift over half an hour. In that period vortices evolve in intensity and can vanish or merge with new vortices being produced in other locations. The strongest vortex was observed with a peak $\Delta p_0 = -8.0$ Pa and there was always at least one vortex with $\Delta p_0 = -5.0$ Pa within the 100 km² domain.

6.2 MEDA and model comparison

We positioned 400 synthetic stations at regular distances covering the simulation domain and analyzed the pressure time-series at each station using the same algorithm used for MEDA including the analysis of data from multiple time windows. The 400 stations operating over the period of the simulation examined are representative of 400 sols at noon with a total analysis time of 200 hours. This number is comparable to our analysis of MEDA data at noon for 415 sols, which accumulates 242 hr of observations for the 12:00-13:00 time range.

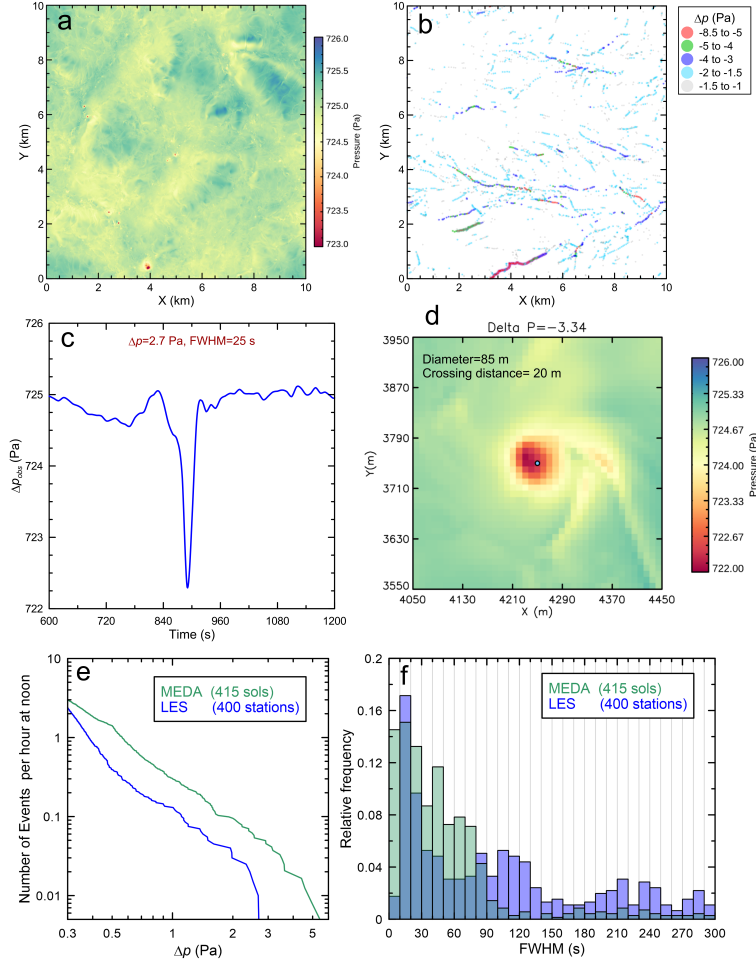


Figure 14. LES simulation of Jezero convective period at noon for $L_s=45^\circ$. (a) Snapshot of the pressure field in the simulation showing intense vortices. (b) Tracks of the most intense vortices. (c) Highest pressure drop identified by the MEDA algorithm. (d) The same vortex in the LES with its true parameters. The large pixels in this image correspond to the spatial resolution of 10 m in the simulation. (e) Comparison of the number of events per hour detected in MEDA data and LES at noon. (f) Relative frequency of both distributions as a function of the vortex detection FWHM.

The most intense pressure drop found with the MEDA algorithm in the LES corresponded to an event of only $\Delta p = -2.7$ Pa with a FWHM of 25s. (Figure 14c). The true characteristics of this vortex are shown in Figure 14d. The event is a vortex of 85 m in diameter crossing at a minimum distance of 20 m of the meteorological station with a $\Delta p_0 = -3.35$ Pa. There are many other more intense vortices in the simulations that are never detected, or that are detected as weaker vortices because of the distance at which they approach one of the measurement points. Supplementary Fig. 7 shows some of the most intense vortices in the simulation and how they are perceived by the closest meteorological station.

A systematic comparison of our detections of MEDA vortices and those in the LES analysis is given in Figure 14e. For pressure drops larger than 0.5 Pa, MEDA detects three times as many events per hour at noon as in the simulation. The MEDA data also has stronger events than those found in the equivalent analysis of the LES.

The most intense vortices found at Jezero are comparable to the most intense vortices in the simulation (although they are not identified by any of the 400 synthetic stations). The distribution of the duration of the events is similar for events of 20-30 s, and very different for short and long events (Figure 14f). Short events cannot be examined in the LES, which is limited by its output frequency of 0.1 Hz. The population of long-duration vortices in the LES contrasts with the smaller time durations of most events in MEDA data. In the LES this population is created by the capability in the simulation to detect the passage of distant vortices. In the MEDA pressure data obtained at Jezero, turbulence and noise make detections of distant events more difficult, while the "clean" long pressure drops created by distant vortices in the LES are easier to distinguish.

The LES allows us to examine how many vortices are present at any given time, and in particular, how many intense vortices with the potential to become dusty are produced in the simulation. The probability of a vortex to be dusty at Jezero depends on the intensity of the pressure drop and becomes larger than 66% for events detected with $\Delta p_{obs} = -2.0$ Pa or larger. Over the 1,800 s of the LES, there are 20 vortices active with pressure drops from -1.0 to -8.4 Pa with a mean pressure intensity of -2.0 Pa. This results in a vortex production rate in the simulation of at least $0.2 \text{ events km}^{-2}$ at noon (with $\Delta p_{obs} < -2.0$ Pa). Since MEDA data shows 3 times as much activity, the production rate of comparable vortices in MEDA data is 0.6 km^{-2} at noon. These events are nearly always dusty in MEDA data. In addition, the integrated vortex and DD activity over a sol can be 3-4 times larger than the peak activity at noon, scaling to a DD production rate at Jezero of $\sim 1.8 - 2.4 \text{ DD km}^{-2} \text{ sol}^{-1}$. This estimation is in agreement with an independent estimation of the DD production rate at Jezero of $2.0 \text{ DD km}^{-2} \text{ sol}^{-1}$ (Toledo et al., 2022), which is based on a combination of the frequency of DDs detected with the RDS Top detectors, the estimated diameters of vortices from the duration of RDS variations, the average winds, and the range of times the vortices are expected to be active (Toledo et al., 2022).

7 Discussion

7.1 Density of dust devils at Jezero

Our analysis of the LES illustrates the difficulties to observe the very close passages of vortices. In our model fits to selected MEDA vortices we observed the close passages of several DDs at distances much smaller than the vortex radius. Statistically, these are infrequent events that produce intense pressure drops and that in our sample of MEDA vortices were DDs that carried significant amounts of dust. Here we investigate the statistical significance of these close passing DDs.

We model the trajectories of vortices randomly launched in a two-dimensional box of $10 \times 10 \text{ km}^2$ assuming a vortex production rate, ρ_v , defined as the number of dust devils per square kilometer and sol. We consider that vortices can survive active during a time $t_v = 0.66 \times (D)^{\frac{2}{3}}$, where D is the vortex diameter and t_v is given in minutes (Lorenz, 2013). Vortices with diameters of 20-40 m survive 5-7.5 minutes and we assume a fixed surviving time of 7.5 minutes. We also assume a vortex drift of $V_v = 5 \text{ ms}^{-1}$ from average wind speeds measured during daytime at Jezero (Rodriguez-Manfredi et al., 2022). We examine trajectories replicating 415 sols of data with measurements for 50% of the time. The trajectory of each individual vortex is integrated over 7.5 minutes measuring its closest approach to the center regardless of any distribution of diameters. For each simulated sol we identify the closest approach to the center of the domain and we count how many vortices pass at a range of distances from 10 to 500 m. We perform 15-25 Monte-Carlo simulations of the whole process for each value of ρ_v to obtain statistical values (each Monte-Carlo simulation implying the integration in time of $\rho_v \times 100 \times 415/2$ vortex trajectories).

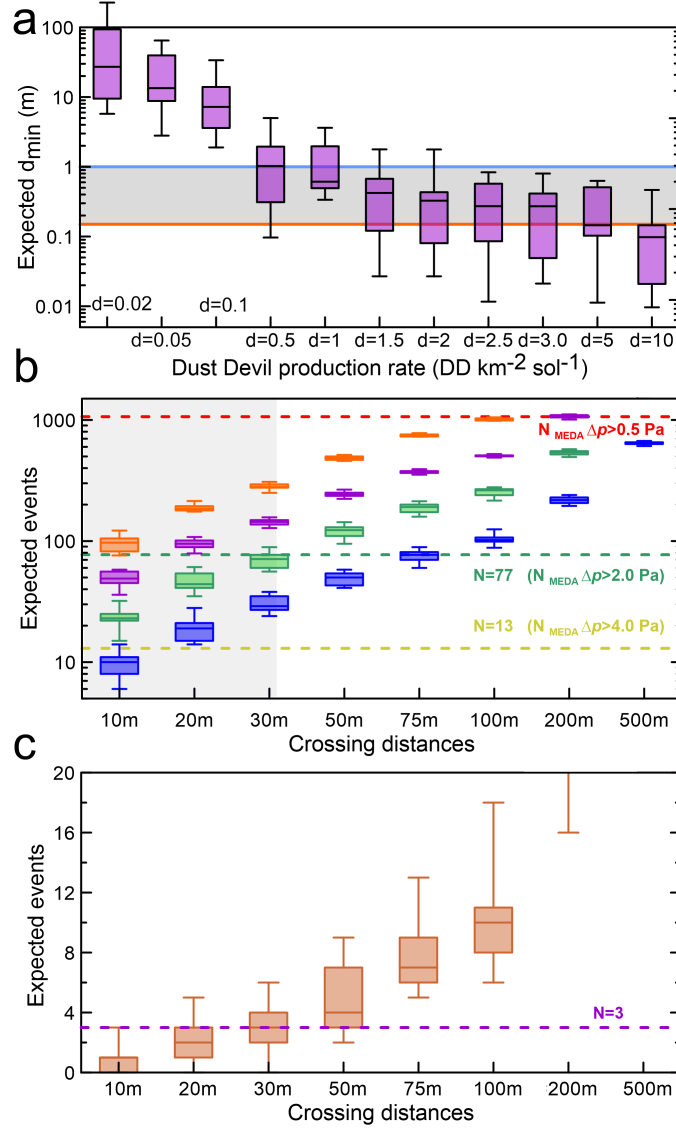


Figure 15. Monte Carlo simulations of trajectories for different DD production rates. (a) Whisker box plot of the minimum crossing distance of a population of vortices produced by Monte-Carlo simulations with production rates of 0.02-10.0 DDs $\text{km}^{-2} \text{sol}^{-1}$. For each production rate the box shows the distribution of values organized in quartiles with the median being the central horizontal line. Long horizontal lines show minimum distances of 0.15m and 1.0 m and the dashed area is the region to fit. (b) Whisker box plot of the number of vortices that would cross at different minimum distances of MEDA for values of ρ_v from 1.0 (blue), 2.5 (green), 5.0 (purple) and 10.0 (orange), all in units of DDs $\text{km}^{-2} \text{sol}^{-1}$. Horizontal lines show the number of detections in MEDA data of pressure drops with at least 4.0 Pa (yellow green), 2.0 Pa (green), and 0.5 Pa (red). (c) Whisker box plot of the number of vortices that would cross at minimum distances for $\rho_v=0.1$ DDs $\text{km}^{-2} \text{sol}^{-1}$. The horizontal line highlights the three 100-m size DDs observed at a minimum distance of 30 m.

637
638

The DD with the closest approach to Perseverance was the one in sol 82, with a modeled minimum approach of 0.15 m. To take into account possible uncertainties

in the minimum distance of the modeled vortices we consider that this minimum approach could be as high as 1.0 m. We examine our simulations to determine which DD production rate is compatible with this observation. Figure 15a shows a whisker plot of these simulations. In order to have a single vortex crossing a distance of Perseverance of 0.15-1.0 m, a dust devil production rate of 0.5-5.0 DD km⁻²sol⁻¹ is needed, with the best results found for 3.0 DD km⁻²sol⁻¹. Smaller vortex survival times than the one assumed would require higher DD production rates.

Figure 15b shows the number of events in simulations with different production rates that cross at different distances to the MEDA sensors. This is compared with the number of vortices detected for different pressure drop thresholds. A DD production rate of 2.5 DDs km⁻²sol⁻¹ is compatible with detected pressure drops in MEDA data of 2.0 Pa (most of them being dusty at Jezero) being caused by more intense vortices crossing at distances of about 30 m or smaller. The very large number of vortices detected in MEDA with $\Delta p_{obs} > 0.5$ Pa cannot be fitted by this production rate, and requires the more frequent formation of vortices of smaller intensity. Thus, the production rate of small intensity vortices must be substantially larger than the 2.5 DDs km⁻²sol⁻¹ that we consider can fit the intense vortices that we detect with values of about 2.0 Pa and that tend to be dusty.

In addition, there are three DDs in the MEDA observations with a diameter of 87-135 m crossing at distances of about 30 m. Figure 15c shows results of our Monte-Carlo simulation of trajectories considering a dust devil production rate of DDs of this size category of 0.1 DD km⁻²sol⁻¹. This simulation fits the number of encounters of large vortices at 30 m. This implies that vortices with diameters of 100 m are produced at Jezero 25 times less frequently than the vortices that we detect with a mean diameter of 20 m.

When putting together our results, we find that for typical dust devil sizes of 20 m in diameter, DD production rates of 2.0-3.0 DD km⁻²sol⁻¹ are reasonable values. This range of values is comparable to other studies at Jezero (Toledo et al., 2022), and smaller than the largest values found at some other locations on Mars that range from 7-15 DD km⁻²sol⁻¹ from analysis of DD surveys in images obtained by Pathfinder cameras (Ferri et al., 2003; Metzger et al., 1999), to 50 DD km⁻²sol⁻¹ from Spirit during a season of high DD activity (Ls=173-340°) (Greeley et al., 2006, 2010; Ferri et al., 2003; Waller, 2011). In many other locations, like Gale crater, the dust devils production rate is much smaller (Ordóñez-Etxeberria et al., 2020), or negligible, like in the location of Insight in Elysium Planitia (Spiga et al., 2021). While vortices in Jezero are very frequently dusty, the observed activity is not beyond what has been observed in the past.

7.2 Intense vortices and risks to surface hardware

The WS has two booms. Each boom is made of 6 transducer boards that include redundant elements. In each transducer board hot and cold dices are connected to the board by sub-mm diameter filaments (Rodriguez-Manfredi et al., 2021). Over the course of the mission two failures in the boards were detected at the same time as encounters with DDs. The DD on sol 313 was the 13th dustiest event detected and the DD on sol 413 was the 4th dustiest. The characteristics of these events are summarized in Table 2.

The first event occurred during the dust storm period and affected the WS boom 2. Supplementary Fig. S8 shows images of the WS and MEDA measurements obtained during passage of this DD. The delay between the peak pressure drop and the largest decrease in light measured by RDS Top 7 suggest this was not a direct impact with the vortex, but a more tangential one. Wind measurements obtained just before the WS failure peaked at values of 22 ms⁻¹, which are on the same level as the peak winds

Table 2. Vortices implied in Wind Sensors damage.

Sol	LTST	Δp_{obs} (Pa)	Rank (Δp_{obs})	FWHM (s)	RDSTop7 (%)	Rank (RDSTop7)	WS peak (ms^{-1})
313	13:42:14	1.8	95	36	9	13	22
413	14:22:26	4.0	13	13	20	4	–

observed in the most intense vortices detected in the MEDA data set. All this factors suggest a vortex passage at a distance comparable to the vortex radius, which would be coincident with the strongest winds in the vortex. Using equation (1) to invert the value of the central pressure drop, this would require a vortex with a central pressure drop of at least 7 Pa. If the vortex impacted Perseverance at a distance larger than its radius, then the dust devil could have been substantially more intense carrying larger size grains. Because we only have wind information during the approach phase we cannot retrieve the physical parameters of this vortex using the vortex drift model.

The second wind sensor failure that can be linked to a DD occurred on sol 413. The event had a detected pressure drop of 4.0 Pa and a high dust content with a 20% reduction of irradiance measured by RDS. Although wind measurements were obtained during the vortex encounter, examining their values requires a new retrieval process that takes into account the functional boards at the time. Because the central pressure drop and event duration are typical of the very close approaches, and the dustiness of the vortex measured by RDS is high, we expect that this was a very close approach of an intense dust devil in Jezero with a likely size close to the most common vortices with diameters of $\sim 17 \pm 8$ m.

7.3 Contribution of vortices to dust-lifting at Jezero

Greeley et al. (2006) computed the average dust flux to the atmosphere transported by dust devils in Gusev crater from images obtained by the Spirit cameras. Vertical velocities in the dust devils had a mean value of 1.8 ms^{-1} , and dust devils transported an average dust flux of $2.1 \times 10^{-5} \text{ kg m}^{-2} \text{ s}^{-1}$. However this number could vary over several orders of magnitude for individual vortices and seasons.

MEDA offers information on the dust content of individual vortices from RDS data. However, its interpretation is subject to geometrical effects associated with the vortex size, crossing distance and vortex path relative to the Sun. Thus, an unbiased quantification of how much dust each DD transports is not straight-forward. If we also consider the DD longevity relation from Lorenz (2013), then, the largest DD in the MEDA observations, i.e., the DD on sol 213 with a 135 m diameter, can lift 45% of all the dust lifted by the 22 events that we have fitted.

If we assume for estimative purposes that the very uncertain average values of vertical velocity and dust flux found at Gusev crater by Greeley et al. (2006) may also be used for Jezero, then the vortex on sol 213 could potentially raise 300 kg of dust to the atmosphere over a life time of 1,000 s. If vortices at Jezero have a mean diameter of 17 m, as calculated from the closest passing vortices, that means that individual vortices can lift about 1.4 kg of dust each. A dust devil production rate of events of this size of $2.5 \text{ DD km}^{-2} \text{ sol}^{-1}$ would result in a dust flux of $3.5 \text{ kg km}^{-2} \text{ sol}^{-1}$, which is about 20% of the estimates at Gusev crater from Greeley et al. (2006).

The large vortices with sizes of 100 m and a production rate of $0.1 \text{ DD km}^{-2} \text{ sol}^{-1}$ would result in longer-lived vortices with a dust flux of $16 \text{ kg km}^{-2} \text{ sol}^{-1}$.

This means that large vortices dominate the dust flux at Jezero, even though a full calculation of how much dust is being lifted by vortices is not possible with the current data.

8 Conclusions

The rich vortex and DD activity at Jezero, and the multiple atmospheric sensors in MEDA, combine to provide a valuable description of vortices and DDs on Mars. Our main findings in examining these data are:

- Vortices are abundant in Jezero during day-time hours. Their average abundance is 4.9 vortices per sol with a $\Delta p_{obs} > 0.5$ Pa. This number takes into account a renormalization for the portion of time over which MEDA operates. One in every 5 of these vortices carries dust. The daily activity of vortices and dust devils peaks at noon with 1.1 vortices per hour with $\Delta p_{obs} > 0.5$ Pa and 0.25 DDs per hour.
- Nighttime pressure drops similar to those caused by daytime vortices are rare but do exist. Some cases can be caused by convective plumes from the RTG and are accompanied by high temperatures. Other cases do not seem related with the RTG and should be caused by the environment. Additional long pressure drops are observed during the day and can be highly variable, potentially indicative of the passage of convective cells.
- The seasonal evolution of vortices and dust devils over $L_s=6-213^\circ$ is small, but there are clear changes at the end of the Summer and early Autumn with a more spread activity in local time of sol that preserves an overall vortex activity of 4-5 vortices per sol. The seasonal variation of vortices occurs in parallel to changes in the vertical thermal gradient of the atmosphere, which is small until the arrival of the Autumn (Manguira et al., 2022).
- DDs became very frequent during the first sols of a dust storm that affected Jezero at $L_s=152^\circ$. These sols had warmer air temperatures and lower surface to air temperature differences than in previous sols. Vortex activity was inhibited a few sols later accompanying a reduction in the temperature of the air and surface with a gradual increase to the seasonal vertical thermal gradient.
- There is a strong correlation between the intensity of the vortex from the detected pressure drop, and its dust content. Most of the vortices with $\Delta p >$ than 2.0 Pa were dusty. The strongest decrease in RDS Top 7 was caused by a long and intense pressure drop that resulted in a light reduction of 26% ($\Delta\tau$ increase of 0.3). This was caused by a close encounter at 30 m of a DD with a diameter of 135 m.
- Clusters of vortices and DDs are related to the terrain properties. The most intense vortices are found over terrains with relatively low thermal inertia ($TI \approx 300$). There is a strong correlation between the local vertical thermal gradient and the intensity of the vortices. Some intense and large vortices are found over terrains with relatively high thermal inertia and small vertical thermal gradients. We suggest that these events could have formed over different terrains and moved over the location where they are detected.
- A comparison of vortex activity at Jezero with a LES calculated for $L_s=45^\circ$ shows similar characteristics, although MEDA measurements of vortex activity suggest three times higher activity at Jezero than the simulation. The LES allows to examine biases from a meteorological station that has a low probability of finding very close events. The comparison of MEDA data and the LES suggests a dust devil production rate of $1.8 - 2.4$ DD $\text{km}^{-2} \text{sol}^{-1}$.
- MEDA pressure and wind data allow us to fit models of vortices that were applied over DDs causing intense pressure drops. These fits result in vortex

diameters from 5 to 135 m. The DDs with the closest trajectories to Perseverance have a mean diameter of 17 m and the mean diameter of all vortices that we could fit to models was 34 m. Model fits predict that at least one of the vortices detected had a central pressure drop of 9.0 Pa, similar to the most intense vortices observed at Elysium Planitia (Spiga et al., 2021).

- The abundance of DDs passing Perseverance at very close distances results in a vortex formation rate at Jezero of 2.0-3.0 DDs $\text{km}^{-2} \text{sol}^{-1}$. A comparison of this formation rate with the number of vortices detected in MEDA data suggests that vortices with pressure drops of 2.0 Pa, which are generally dusty, correspond to the approach of stronger vortices observed at a distance that in most cases is smaller than 30 m.
- At least three large DDs with diameters of 100 m passed within 30 m of Perseverance. This implies a vortex formation rate for events of this size of 0.1 DDs $\text{km}^{-2} \text{sol}^{-1}$. The comparison with the formation rate of smaller DDs implies that the total dust lifting by vortices at Jezero is dominated by the activity of the larger vortices.

Future analyses of Perseverance observations of DDs combining MEDA data and images will unveil new characteristics of the DD phenomenology in Jezero. New observations over different seasons and terrains, exploring properties such as surface roughness and particle size and cohesion from surface images, will help to understand the characteristics that make Jezero so active in developing DDs within its rich population of convective vortices.

Acknowledgments

We are very grateful to the entire Mars 2020 science operations team. This work has been supported by Grant PID2019-109467GB-I00 funded by MCIN/AEI/10.13039/501100011033/ and by Grupos Gobierno Vasco IT1366-19 and Grupos Gobierno Vasco IT1742-22 and by the Spanish National Research, Development and Innovation Program, through the grants RTI2018-099825-B-C31, ESP2016-80320-C2-1-R and ESP2014-54256-C4-3-R. M. Lemmon is supported by contract 15-712 from Arizona State University and 1607215 from Caltech-JPL. A. Vicente-Retortillo is supported by the Spanish State Research Agency (AEI) Project No. MDM-2017-0737 Unidad de Excelencia “María de Maeztu”- Centro de Astrobiología (INTA-CSIC), and by the Comunidad de Madrid Project S2018/NMT-4291 (TEC2SPACE-CM). Germán Martínez acknowledges JPL funding from USRA Contract Number 1638782. Part of the research was carried out at the Jet Propulsion Laboratory, California Institute of Technology, under a contract with the National Aeronautics and Space Administration (80NM0018D0004). Finnish researchers acknowledge the Academy of Finland grant 328 310529. Researchers based in France acknowledge support from CNES for their work on Perseverance. Baptiste Chide is supported by the Director’s Postdoctoral Fellowship from the Los Alamos National Laboratory.

Open Research

The Mars Environmental Dynamics Analyzer (MEDA) Experiment Data Record (EDR) and Reduced Data Record (RDR) Data Products Archive Bundle (J.A.Rodriguez-Manfredi et al. 2021, The Mars Environmental Dynamics Analyzer, MEDA, NASA Planetary Data System) are available with the following doi: 10.17189/1522849, and can be downloaded from the NASA PDS (https://pds-atmospheres.nmsu.edu/data_and_services/atmospheres.data/PERSEVERANCE/meda.html). The analysis here presented is based on programs written in IDL and Fortran and available at Zenodo at the following link <https://zenodo.org/record/6958141> with doi: 10.5281/zenodo.6958141.

References

- Apestigue, V., Gonzalo, A., Jiménez, J., Boland, J., Lemmon, M., de Mingo, J., ... Arruego, I. (2022, April). Radiation and Dust Sensor for Mars Environmental Dynamic Analyzer Onboard M2020 Rover. *Sensors*, 22(8), 2907. doi: 10.3390/s22082907
- Balme, M., & Greeley, R. (2006, September). Dust devils on Earth and Mars. *Reviews of Geophysics*, 44(3), RG3003. doi: 10.1029/2005RG000188
- Banfield, D., Spiga, A., Newman, C., Forget, F., Lemmon, M., Lorenz, R., ... Banerdt, W. B. (2020, February). The atmosphere of Mars as observed by InSight. *Nature Geoscience*, 13(3), 190-198. doi: 10.1038/s41561-020-0534-0
- Basu, S., Richardson, M. I., & Wilson, R. J. (2004, November). Simulation of the Martian dust cycle with the GFDL Mars GCM. *Journal of Geophysical Research (Planets)*, 109(E11), E11006. doi: 10.1029/2004JE002243
- Chatain, A., Spiga, A., Banfield, D., Forget, F., & Murdoch, N. (2021, November). Seasonal Variability of the Daytime and Nighttime Atmospheric Turbulence Experienced by InSight on Mars. *Geophys. Res. Lett.*, 48(22), e95453. doi: 10.1029/2021GL095453
- Ellehoj, M. D., Gunnlaugsson, H. P., Taylor, P. A., Kahanpää, H., Bean, K. M., Cantor, B. A., ... Whiteway, J. (2010, April). Convective vortices and dust devils at the Phoenix Mars mission landing site. *Journal of Geophysical Research (Planets)*, 115(E8), E00E16. doi: 10.1029/2009JE003413
- Farley, K. A., Williford, K. H., Stack, K. M., Bhartia, R., Chen, A., de la Torre, M., ... Wiens, R. C. (2020, December). Mars 2020 Mission Overview. *Space Sci. Rev.*, 216(8), 142. doi: 10.1007/s11214-020-00762-y
- Fenton, L., Reiss, D., Lemmon, M., Marticorena, B., Lewis, S., & Cantor, B. (2016, November). Orbital Observations of Dust Lofted by Daytime Convective Turbulence. *Space Sci. Rev.*, 203(1-4), 89-142. doi: 10.1007/s11214-016-0243-6
- Ferguson, R. L., Christensen, P. R., & Kieffer, H. H. (2006, December). High-resolution thermal inertia derived from the Thermal Emission Imaging System (THEMIS): Thermal model and applications. *Journal of Geophysical Research (Planets)*, 111(E12), E12004. doi: 10.1029/2006JE002735
- Ferri, F., Smith, P. H., Lemmon, M., & Rennó, N. O. (2003, December). Dust devils as observed by Mars Pathfinder. *Journal of Geophysical Research (Planets)*, 108(E12), 5133. doi: 10.1029/2000JE001421
- Greeley, R., Waller, D. A., Cabrol, N. A., Landis, G. A., Lemmon, M. T., Neakrase, L. D. V., ... Whelley, P. L. (2010, September). Gusev Crater, Mars: Observations of three dust devil seasons. *Journal of Geophysical Research (Planets)*, 115(E8), E00F02. doi: 10.1029/2010JE003608
- Greeley, R., Whelley, P. L., Arvidson, R. E., Cabrol, N. A., Foley, D. J., Franklin, B. J., ... Thompson, S. D. (2006, December). Active dust devils in Gusev crater, Mars: Observations from the Mars Exploration Rover Spirit. *Journal of Geophysical Research (Planets)*, 111(E12), E12S09. doi: 10.1029/2006JE002743
- Guzewich, S. D., Lemmon, M., Smith, C. L., Martínez, G., de Vicente-Retortillo, Á., Newman, C. E., ... Zorzano Mier, M.-P. (2019, January). Mars Science Laboratory Observations of the 2018/Mars Year 34 Global Dust Storm. *Geophys. Res. Lett.*, 46(1), 71-79. doi: 10.1029/2018GL080839
- Jackson, B. (2022, January). Vortices and Dust Devils as Observed by the Mars Environmental Dynamics Analyzer Instruments on Board the Mars 2020 Perseverance Rover. *Planet. Sci. J.*, 3(1), 20. doi: 10.3847/PSJ/ac4586
- Kahanpää, H., & Viúdez-Moreiras, D. (2021, May). Modelling martian dust devils using in-situ wind, pressure, and UV radiation measurements by Mars Science Laboratory. *Icarus*, 359, 114207. doi: 10.1016/j.icarus.2020.114207
- Kahre, M. A., Murphy, J. R., & Haberle, R. M. (2006, June). Modeling the Mar-

- 884 tian dust cycle and surface dust reservoirs with the NASA Ames general circula-
 885 tion model. *Journal of Geophysical Research (Planets)*, 111(E6), E06008. doi:
 886 10.1029/2005JE002588
- 887 Kahre, M. A., Murphy, J. R., Newman, C. E., Wilson, R. J., Cantor, B. A., Lem-
 888 mon, M. T., & Wolff, M. J. (2017). The Mars Dust Cycle. In R. M. Haberle,
 889 R. T. Clancy, F. Forget, M. D. Smith, & R. W. Zurek (Eds.), *Asteroids, comets,*
 890 *meteors - acm2017* (p. 229-294). doi: 10.1017/9781139060172.010
- 891 Kurgansky, M. V., Lorenz, R. D., Renno, N. O., Takemi, T., Gu, Z., & Wei, W.
 892 (2016, November). Dust Devil Steady-State Structure from a Fluid Dynamics
 893 Perspective. *Space Sci. Rev.*, 203(1-4), 209-244. doi: 10.1007/s11214-016-0281-0
- 894 Lemmon, M. T., Smith, M., Viudez-Moreiras, D., de la Torre-Juarez, M., Vicente-
 895 Retortillo, A., Munguira, A., ... Toledo, D. (2022). Dust, Sand, and Winds
 896 within an Active Martian Storm in Jezero Crater. *J. Geophys. Res.*, *submitted to*
 897 *this issue*.
- 898 Lorenz, R. (2013, September). The longevity and aspect ratio of dust devils: Effects
 899 on detection efficiencies and comparison of landed and orbital imaging at Mars.
 900 *Icarus*, 226(1), 964-970. doi: 10.1016/j.icarus.2013.06.031
- 901 Lorenz, R. D. (2013, February). Irregular dust devil pressure drops on Earth and
 902 Mars: Effect of cycloidal tracks. *Planet. Space Sci.*, 76, 96-103. doi: 10.1016/j.pss
 903 .2013.01.001
- 904 Lorenz, R. D. (2016). Heuristic estimation of dust devil vortex parameters and
 905 trajectories from single-station meteorological observations: Application to InSight
 906 at Mars. *Icarus*, 271, 326-337. doi: 10.1016/j.icarus.2016.02.001
- 907 Lorenz, R. D., Lemmon, M. T., & Maki, J. (2021, August). First Mars year of
 908 observations with the InSight solar arrays: Winds, dust devil shadows, and dust
 909 accumulation. *Icarus*, 364, 114468. doi: 10.1016/j.icarus.2021.114468
- 910 Lorenz, R. D., & Reiss, D. (2015, March). Solar panel clearing events, dust devil
 911 tracks, and in-situ vortex detections on Mars. *Icarus*, 248, 162-164. doi: 10.1016/
 912 j.icarus.2014.10.034
- 913 Martínez, G. M., Sebastián, E., Vicente-Retortillo, A., Fischer, E., Toledo, D.,
 914 Gómez, F., ... Rodríguez-Manfredi, J. A. (2022, June). Albedo and Thermal
 915 Inertia at Jezero Crater During the First 350 Sols of the Mars 2020 Mission. In
 916 *Seventh international workshop on the mars atmosphere: Modelling and observa-*
 917 *tions* (p. 1510).
- 918 Mason, J. P., Patel, M. R., & Lewis, S. R. (2013, March). Radiative transfer mod-
 919 elling of dust devils. *Icarus*, 223(1), 1-10. doi: 10.1016/j.icarus.2012.11.018
- 920 Metzger, S. M., Carr, J. R., Johnson, J. R., Parker, T. J., & Lemmon, M. T. (1999,
 921 January). Dust devil vortices seen by the Mars Pathfinder Camera. *Geo-*
 922 *phys. Res. Lett.*, 26(18), 2781-2784. doi: 10.1029/1999GL008341
- 923 Munguira, A., Hueso, R., Sánchez-Lavega, A., de la Torre-Juarez, M., Martinez,
 924 G., Newman, C., ... Lorenz, R. (2022, June). Mars 2020 MEDA Measurements
 925 of Near Surface Atmospheric Temperatures at Jezero. In *Seventh international*
 926 *workshop on the mars atmosphere: Modelling and observations* (p. 1509).
- 927 Murdoch, N., Stott, A., Gillier, M., Lemmon, M., Hueso, R., Munguira, A., ... Mi-
 928 moun, D. (2022). First acoustic recordings of a Martian Dust Devil. *Nature*
 929 *Communications*, *submitted*.
- 930 Murphy, J., Steakley, K., Balme, M., Deprez, G., Esposito, F., Kahanpää, H., ...
 931 Whelley, P. (2016, November). Field Measurements of Terrestrial and Martian
 932 Dust Devils. *Space Sci. Rev.*, 203(1-4), 39-87. doi: 10.1007/s11214-016-0283-y
- 933 Neakrase, L. D. V., Balme, M. R., Esposito, F., Kelling, T., Klose, M., Kok, J. F.,
 934 ... Wurm, G. (2016, November). Particle Lifting Processes in Dust Devils.
 935 *Space Sci. Rev.*, 203(1-4), 347-376. doi: 10.1007/s11214-016-0296-6
- 936 Newman, C. E., de la Torre Juárez, M., Pla-García, J., Wilson, R. J., Lewis, S. R.,
 937 Neary, L., ... Rodríguez-Manfredi, J. A. (2021). Multi-model Meteorological and

- 938 Aeolian Predictions for Mars 2020 and the Jezero Crater Region. *Space Sci. Rev.*,
939 *217*(1), 20. doi: 10.1007/s11214-020-00788-2
- 940 Newman, C. E., Hueso, R., Lemmon, M. T., Munguira, A., Álvaro Vicente-
941 Retortillo, Apestigue, V., ... Guzewich, S. D. (2022). The dynamic atmo-
942 spheric and aeolian environment of jezero crater, mars. *Science Advances*,
943 *8*(21), eabn3783. Retrieved from [https://www.science.org/doi/abs/10.1126/](https://www.science.org/doi/abs/10.1126/sciadv.abn3783)
944 [sciadv.abn3783](https://www.science.org/doi/abs/10.1126/sciadv.abn3783) doi: 10.1126/sciadv.abn3783
- 945 Newman, C. E., Lewis, S. R., Read, P. L., & Forget, F. (2002, December). Modeling
946 the Martian dust cycle, 1. Representations of dust transport processes. *Journal of*
947 *Geophysical Research (Planets)*, *107*(E12), 5123. doi: 10.1029/2002JE001910
- 948 Ordóñez-Etxeberria, I., Hueso, R., & Sánchez-Lavega, A. (2020, September). Strong
949 increase in dust devil activity at Gale crater on the third year of the MSL mission
950 and suppression during the 2018 Global Dust Storm. *Icarus*, *347*, 113814. doi:
951 10.1016/j.icarus.2020.113814
- 952 Ordonez-Etxeberria, I., Hueso, R., & Sánchez-Lavega, A. (2018). A systematic
953 search of sudden pressure drops on Gale crater during two Martian years derived
954 from MSL/REMS data. *Icarus*, *299*, 308-330. doi: 10.1016/j.icarus.2017.07.032
- 955 Reiss, D., Fenton, L., Neakrase, L., Zimmerman, M., Statella, T., Whelley, P., ...
956 Balme, M. (2016, November). Dust Devil Tracks. *Space Sci. Rev.*, *203*(1-4),
957 143-181. doi: 10.1007/s11214-016-0308-6
- 958 Rennó, N. O., Burkett, M. L., & Larkin, M. P. (1998, November). A Sim-
959 ple Thermodynamical Theory for Dust Devils. *Journal of Atmospheric Sci-*
960 *ences*, *55*(21), 3244-3252. doi: 10.1175/1520-0469(1998)055<3244:
961 ASTTFD>2.0.CO;2
- 962 Richardson, M. I., Toigo, A. D., & Newman, C. E. (2007, January). PlanetWRF:
963 A general purpose, local to global numerical model for planetary atmospheric and
964 climate dynamics. *Journal of Geophysical Research (Planets)*, *112*(E9), E09001.
965 doi: 10.1029/2006JE002825
- 966 Rodríguez-Manfredi, J., de la Torre Juárez, M., Alonso, A., Apéstigue, V., Arruego,
967 I., Atienza, T., ... others (2021). The mars environmental dynamics analyzer,
968 meda. a suite of environmental sensors for the mars 2020 mission. *Space Science*
969 *Reviews*, *217*(3), 1–86.
- 970 Rodríguez-Manfredi, J., de la Torre Juárez, M., Sánchez-Lavega, A., Hueso, R., &
971 Martínez, G. e. a. (2022). The rich meteorology of jezero crater over the first 250
972 sols of perseverance on mars. *submitted to Nature Geosci.*
- 973 Ryan, J. A. (1972, December). Relation of dust devil frequency and diameter to
974 atmospheric temperature. *J. Geophys. Res.*, *77*(36), 7133-7137. doi: 10.1029/
975 JC077i036p07133
- 976 Ryan, J. A., & Lucich, R. D. (1983, December). Possible dust devils, vortices on
977 Mars. *J. Geophys. Res.*, *88*, 11005-11011. doi: 10.1029/JC088iC15p11005
- 978 Sánchez-Lavega, A., del Río-Gaztelurrutia, T., Hueso, R., & de la Torre, M. (2022).
979 Perseverance studies of the Martian atmosphere over Jezero from pressure mea-
980 surements). *J. Geophys. Res.*, *submitted to this issue*.
- 981 Spiga, A., Murdoch, N., Lorenz, R., Forget, F., Newman, C., Rodríguez, S., ...
982 Banerdt, W. B. (2021, January). A Study of Daytime Convective Vortices and
983 Turbulence in the Martian Planetary Boundary Layer Based on Half-a-Year of
984 InSight Atmospheric Measurements and Large-Eddy Simulations. *Journal of*
985 *Geophysical Research (Planets)*, *126*(1), e06511. doi: 10.1029/2020JE006511
- 986 Toledo, D., Apéstigue, V., & Arruego, I. (2022). Dust devil frequency of occurrence
987 and radiative effects at Jezero as measured by MEDA Radiation and Dust Sensor
988 (RDS). *J. Geophys. Res.*, *submitted to this issue*.
- 989 Vicente-Retortillo, Á., Martínez, G. M., Lemmon, M., Hueso, R., Johnson, J., Sulli-
990 van, R., ... Rodríguez-Manfredi, J. (2022). Dust Lifting Through Surface Albedo
991 Changes at Jezero Crater, Mars. *Geophys. Res. Lett.*, *submitted to this issue*.

- 992 Vicente-Retortillo, Á., Martínez, G. M., Renno, N., Newman, C. E., Ordonez-
 993 Etxeberria, I., Lemmon, M. T., ... Sánchez-Lavega, A. (2018, December). Sea-
 994 sonal Deposition and Lifting of Dust on Mars as Observed by the Curiosity Rover.
 995 *Scientific Reports*, 8, 17576. doi: 10.1038/s41598-018-35946-8
- 996 Viúdez-Moreiras, D., Newman, C. E., Forget, F., Lemmon, M., Banfield, D., Spiga,
 997 A., ... Grott, M. (2020, September). Effects of a Large Dust Storm in the Near-
 998 Surface Atmosphere as Measured by InSight in Elysium Planitia, Mars. Compari-
 999 son With Contemporaneous Measurements by Mars Science Laboratory. *Journal*
 1000 *of Geophysical Research (Planets)*, 125(9), e06493. doi: 10.1029/2020JE006493
- 1001 Waller, D. (2011). Active dust devils on mars: A comparison of six spacecraft land-
 1002 ing sites. *Arizona State University*.
- 1003 Wu, Z., Richardson, M. I., Zhang, X., Cui, J., Heavens, N. G., Lee, C., ... Witek,
 1004 M. (2021, September). Large Eddy Simulations of the Dusty Martian Convective
 1005 Boundary Layer With MarsWRF. *Journal of Geophysical Research (Planets)*,
 1006 126(9), e06752. doi: 10.1029/2020JE006752